

Evaporation and condensation of a binary mixture of vapors on a plane condensed phase: Numerical analysis of the linearized Boltzmann equation

Shugo Yasuda, Shigeru Takata,^{a)} and Kazuo Aoki

Department of Aeronautics and Astronautics and Advanced Research Institute of Fluid Science and Engineering, Graduate School of Engineering, Kyoto University, Kyoto 606-8501, Japan

(Received 4 August 2004; accepted 1 February 2005; published online 31 March 2005)

Half-space problem of evaporation and condensation of a binary mixture of vapors is investigated on the basis of the linearized Boltzmann equation for hard-sphere molecules with the complete condensation condition. The problem is analyzed numerically by a finite-difference method, in which the complicated collision integrals are computed by the extension of the method proposed by Y. Sone, T. Ohwada, and K. Aoki [“Temperature jump and Knudsen layer in a rarefied gas over a plane wall: Numerical analysis of the linearized Boltzmann equation for hard-sphere molecules,” *Phys. Fluids A* **1**, 363 (1989)] to the case of a gas mixture. As a result, the behavior of the mixture is clarified not only at the level of the macroscopic quantities but also at the level of the velocity distribution function. In addition, accurate formulas of the temperature, pressure, and concentration jumps caused by the evaporation and condensation are constructed for arbitrary values of the concentration of the background reference state by the use of the Chebyshev polynomial approximation. © 2005 American Institute of Physics. [DOI: 10.1063/1.1882252]

I. INTRODUCTION

It is widely accepted that gas flows under the ordinary pressure are well described by the Navier–Stokes set of equations. This is the fundamental set to the conventional fluid dynamics, which is composed of the mass, momentum, and energy conservation laws with Newton’s law for the stress and Fourier’s law for the heat flow.¹ Gas flows around a body are usually studied by the Navier–Stokes set with the nonslip condition for the flow velocity and the nonjump condition for the temperature at the surface of the body. However, such conditions are invalid if the phase transition (evaporation and/or condensation) takes place at the surface of the body, i.e., if vapor flows around condensed phases are considered. In fact, it is known that there is a difference of the temperature between the surface of the condensed phase and the gas at the surface. The same is true for the pressure: the pressure of the vapor at the surface is different from its saturation pressure at the temperature of the surface. These differences are called the jump of temperature and that of pressure, respectively.² In order to study gas flows with the phase transition by the fluid-dynamic set, one needs boundary conditions that describe these jumps correctly. Such conditions are sometimes called the jump conditions for evaporation and condensation.

When evaporation or condensation takes place, the vapor (gas phase) and its condensed phase (liquid phase) are not in equilibrium, so that the assumption of the local equilibrium state is violated at the interface of different phases. Hence, the conventional fluid dynamics must be supplemented there by another principle that is free from the local-equilibrium assumption. This causes those studies of the jump condition

that are based on the irreversible thermodynamics and on the kinetic theory of gases (e.g., Refs. 3–8 and references therein). The present study falls into the latter category.

In kinetic theory, the analysis of the jump for evaporation and condensation is finally reduced to a half-space boundary-value problem of the Boltzmann equation. Physically it is a problem of a steady vapor flow condensing on or evaporating from its plane condensed phase that is in a uniform equilibrium state at a far distance. The problem is seen to be solved only conditionally, and the solvable condition, which is to be given as certain relations among the parameters, gives the jump conditions for the fluid-dynamic equations. When evaporation or condensation is strong, the problem is for the nonlinear Boltzmann equation and the obtained jump conditions are for the compressible Euler set of equations. When evaporation or condensation is weak, the problem is for the linearized Boltzmann equation and the obtained jump conditions are for the (incompressible) Navier–Stokes or Stokes set of equations. The reader is referred to Refs. 6 and 9–11 for information about this issue in the case of a single-species vapor, in which the correspondence between the nonlinear Boltzmann and Euler systems and that between the linearized Boltzmann and Navier–Stokes (or Stokes) systems are established by a systematic asymptotic analysis of the Boltzmann system for small Knudsen numbers. In the case of a mixture of vapors, although there is no appropriate literature for the general description, it is possible to show that the same correspondences are true. In the present paper, we will investigate the half-space problem for the linearized Boltzmann equation, in order to provide the jump conditions at the surface of the condensed phase for the Navier–Stokes or Stokes equations, in the case of a mixture of two species vapors.

^{a)}Electronic mail: takata@aero.mbox.media.kyoto-u.ac.jp

The present paper may be considered as a continuation of our recent papers^{12–14} on the half-space problems of the linearized Boltzmann equation for a mixture. We will establish an accurate numerical solution of the present problem by means of the finite-difference method developed in Refs. 12–14. It is an extension of the method in Ref. 15 to gas mixtures. As before, we carry out the analysis for the hard-sphere model, which is the most fundamental molecular model in kinetic theory, and provide the accurate data for arbitrary values of the concentration (the number fraction of a component species) of the background reference equilibrium state. The data will serve as the standard to assess other approximation methods that mainly aim at the practical use with a more realistic molecular model.

Before moving on to the following section, here we shall remark on two things. The first one is on the relation of the linearized problem to the nonlinear one. One may naturally think that the solution of the former would be an approximate solution of the latter if the evaporation or condensation is weak. However it is not true. According to the comprehensive studies for a single-species vapor, the jump conditions obtained from the linearized problem has a common structure to evaporation and condensation, while those from the nonlinear problem has a qualitatively different structure between evaporation and condensation.^{16–22} That is, there is a discrepancy between the linearized and nonlinear problems. This discrepancy was resolved by Sone by means of a weakly nonlinear analysis for weak evaporation or condensation.^{6,23} According to his result, although the linearized problem provides a correct approximation to the nonlinear problem for evaporation, it fails to approximate the latter for condensation. The same is true in the case of a mixture of vapors.²⁴ Because of this failure, the solution of the linearized problem is meaningless for condensation as a certain approximation to that of the nonlinear one. Nevertheless, we should stress that, as mentioned above in the third paragraph, the linearized problem plays an essential role to determine the jump conditions for evaporation and condensation for the Navier–Stokes or Stokes equations. The linearized problem itself has a physical significance, independent of the nonlinear one. This is why the linearized problem is studied here.

The second is on the jump conditions for slightly rarefied gases. In a slightly rarefied gas, where the Knudsen number (the ratio of the mean free path to the reference length) is small, the jump occurs not only on the surface of the condensed phase but also on the surface of a simple rigid solid body as a gas rarefaction effect. The sources of such a jump are the gradients of temperature and concentration normal to the surface, the curvature of the surface, and so on. Among them, the jump caused by the gradients of temperature and concentration^{25–27} are often studied by kinetic theory because they occur as the first correction, superior to the others, to the nonjump condition of the temperature on the simple solid surface. On the surface of the condensed phase, however, it is seen that the jump due to these effects is in general smaller (i.e., of the higher order in the Knudsen number) than that caused by the evaporation and condensation. The latter is the jump studied in the present paper.

II. FORMULATION OF THE PROBLEM

A. Problem

We consider a semi-infinite expanse of a binary mixture of vapors, species A and B , bounded by a plane condensed phase at rest. The condensed phase is a homogeneous mixture of the liquid of species A and that of B with a constant uniform temperature T_0 , and its surface is located at $X_1=0$, where X_i is the rectangular coordinate system. The mixture occupies the region $X_1>0$, and, at a far distance from the surface, it is in the equilibrium state characterized by the pressure $p_0(1+P_\infty)$, temperature $T_0(1+\tau_\infty)$, and flow velocity $(2kT_0/m^A)^{1/2}(u_\infty, 0, 0)$ of the mixture and by the concentration (molecular number fraction) $X_0^A + \chi_\infty^A$ of species A .²⁸ Here p_0 is the saturation pressure of the mixture in contact with the condensed phase at temperature T_0 and X_0^A is the concentration of species A in the saturated mixture. In the sequel the Greek letters α and β will be symbolically used to represent the species, i.e., $\{\alpha, \beta\} = \{A, B\}$.

We will investigate the steady behavior of the mixture under the following assumptions: (i) the molecules of vapor α are hard spheres of mass m^α and diameter d^α , and they collide elastically with each other; (ii) the behavior of the mixture is described by the Boltzmann equation with the complete condensation condition for the outgoing molecules from the condensed phase; and (iii) the quantities $|P_\infty|$, $|\tau_\infty|$, $|\chi_\infty^A|$, and $|u_\infty|$ are so small that the equations and boundary conditions can be linearized around the reference equilibrium state at rest characterized by the temperature T_0 and pressure p_0 of the mixture and by the concentration X_0^A of species A .

B. Basic equation and boundary condition

We first summarize the main notation used in the paper. The n_0 is the reference molecular number density of the mixture and is defined by $n_0 = p_0/kT_0$, where k is Boltzmann's constant. The l_0 is the mean free path of the molecules in the equilibrium state at rest with the molecular number density n_0 and temperature T_0 when gas B is absent (i.e., $l_0 = 1/[\sqrt{2}\pi(d^A)^2n_0]$). The x_i is the nondimensional coordinate system defined by $x_i = X_i l_0^{-1}(\sqrt{\pi}/2)^{-1}$. The $(2kT_0/m^A)^{1/2}\zeta_i$ [or $(2kT_0/m^A)^{1/2}\xi$] is the molecular velocity, $n_0(2kT_0/m^A)^{-3/2}(X_0^\alpha + \phi^\alpha)E^\alpha$ is the velocity distribution function of the molecules of species α , where $X_0^B = 1 - X_0^A$ and $E^\alpha(\xi) = (\hat{m}^\alpha/\pi)^{3/2}\exp(-\hat{m}^\alpha|\xi|^2)$ with $\hat{m}^\alpha = m^\alpha/m^A$. The ratio of molecular diameters $\hat{d}^\alpha = d^\alpha/d^A$ will also be used. The molecular number density, pressure, temperature, flow velocity, stress tensor, and heat-flow vector of species α are denoted, respectively, by $n_0(X_0^\alpha + N^\alpha)$, $p_0(X_0^\alpha + P^\alpha)$, $T_0(1 + \tau^\alpha)$, $(2kT_0/m^A)^{1/2}u_i^\alpha$, $p_0(X_0^\alpha\delta_{ij} + P_{ij}^\alpha)$, and $p_0(2kT_0/m^A)^{1/2}Q_i^\alpha$, where δ_{ij} is Kronecker's delta. Those of the mixture are denoted by $n_0(1 + N)$, $p_0(1 + P)$, $T_0(1 + \tau)$, $(2kT_0/m^A)^{1/2}u_i$, $p_0(\delta_{ij} + P_{ij})$, and $p_0(2kT_0/m^A)^{1/2}Q_i$.

The linearized Boltzmann equation in the present case ($\partial/\partial t = \partial/\partial x_2 = \partial/\partial x_3 = 0$) is written as^{29–31}

$$\zeta_1 \frac{\partial \phi^\alpha}{\partial x_1} = \sum_{\beta=A,B} K^{\beta\alpha} \tilde{L}^{\beta\alpha} (X_0^\alpha \phi^\beta, X_0^\beta \phi^\alpha), \quad (1)$$

where $\tilde{L}^{\beta\alpha}$ is the linearized collision integral defined by

$$\begin{aligned} \tilde{L}^{\beta\alpha}(f, g) &= \frac{1}{4\sqrt{2\pi}} \int [f(\boldsymbol{\zeta}') - f(\boldsymbol{\zeta}_*) + g(\boldsymbol{\zeta}') - g(\boldsymbol{\zeta})] E^\beta(\boldsymbol{\zeta}_*) \\ &\quad \times |\mathbf{e} \cdot \hat{\mathbf{V}}| d\Omega(\mathbf{e}) d^3\boldsymbol{\zeta}_*, \end{aligned} \quad (2)$$

with

$$\boldsymbol{\zeta}' = \boldsymbol{\zeta} + \frac{\hat{\boldsymbol{\mu}}^{\beta\alpha}}{\hat{m}^\alpha} (\mathbf{e} \cdot \hat{\mathbf{V}}) \mathbf{e}, \quad \boldsymbol{\zeta}'_* = \boldsymbol{\zeta}_* - \frac{\hat{\boldsymbol{\mu}}^{\beta\alpha}}{\hat{m}^\beta} (\mathbf{e} \cdot \hat{\mathbf{V}}) \mathbf{e}, \quad (3a)$$

$$\hat{\mathbf{V}} = \boldsymbol{\zeta}_* - \boldsymbol{\zeta}, \quad d^3\boldsymbol{\zeta}_* = d\zeta_{*1} d\zeta_{*2} d\zeta_{*3}, \quad (3b)$$

$$K^{\beta\alpha} = \left(\frac{\hat{d}^\alpha + \hat{d}^\beta}{2} \right)^2, \quad \hat{\boldsymbol{\mu}}^{\beta\alpha} = \frac{2\hat{m}^\alpha \hat{m}^\beta}{\hat{m}^\alpha + \hat{m}^\beta}. \quad (3c)$$

Here \mathbf{e} is a unit vector, $\boldsymbol{\zeta}_*$ the variable of integration corresponding to $\boldsymbol{\zeta}$, and $d\Omega(\mathbf{e})$ the solid-angle element in the direction of \mathbf{e} . The integration in Eq. (2) is carried out over the whole space of $\boldsymbol{\zeta}_*$ and over all the directions of \mathbf{e} .

The complete condensation condition at the surface of the condensed phase ($x_1=0$) is written as

$$\phi^\alpha = 0, \quad \zeta_1 > 0, \quad (4)$$

and the condition at a far distance from the surface ($x_1 \rightarrow \infty$) is written as

$$\phi^\alpha \rightarrow \phi_\infty^\alpha = X_0^\alpha P_\infty + \chi_\infty^\alpha + 2\hat{m}^\alpha X_0^\alpha \zeta_1 u_\infty + \left(\hat{m}^\alpha \zeta_1^2 - \frac{5}{2} \right) X_0^\alpha \tau_\infty, \quad (5)$$

where $\chi_\infty^B = -\chi_\infty^A$ (see the end of the next paragraph).

The macroscopic quantities N^α , u_i^α , etc., of species α are written in terms of ϕ^α as

$$N^\alpha = \int \phi^\alpha E^\alpha d^3\boldsymbol{\zeta}, \quad (6a)$$

$$u_i^\alpha = \frac{1}{X_0^\alpha} \int \zeta_i \phi^\alpha E^\alpha d^3\boldsymbol{\zeta}, \quad (6b)$$

$$\tau^\alpha = \frac{2}{3} \frac{1}{X_0^\alpha} \int \left(\hat{m}^\alpha \zeta_j^2 - \frac{3}{2} \right) \phi^\alpha E^\alpha d^3\boldsymbol{\zeta}, \quad (6c)$$

$$P^\alpha = \frac{2}{3} \hat{m}^\alpha \int \zeta_j^2 \phi^\alpha E^\alpha d^3\boldsymbol{\zeta} (= N^\alpha + X_0^\alpha \tau^\alpha), \quad (6d)$$

$$P_{ij}^\alpha = 2\hat{m}^\alpha \int \zeta_i \zeta_j \phi^\alpha E^\alpha d^3\boldsymbol{\zeta}, \quad (6e)$$

$$Q_i^\alpha = \hat{m}^\alpha \int \zeta_i \zeta_j^2 \phi^\alpha E^\alpha d^3\boldsymbol{\zeta} - \frac{5}{2} X_0^\alpha u_i^\alpha. \quad (6f)$$

Here and henceforth, unless otherwise stated, the integration with respect to $\boldsymbol{\zeta}$ is performed over its whole space. The macroscopic quantities of the mixture are expressed in terms of those of component species as

$$N = \sum_{\beta=A,B} N^\beta, \quad P = \sum_{\beta=A,B} P^\beta, \quad (7a)$$

$$u_i = \left(\sum_{\beta=A,B} \hat{m}^\beta X_0^\beta u_i^\beta \right) / \left(\sum_{\beta=A,B} \hat{m}^\beta X_0^\beta \right), \quad (7b)$$

$$\tau = \sum_{\beta=A,B} X_0^\beta \tau^\beta, \quad P_{ij} = \sum_{\beta=A,B} P_{ij}^\beta, \quad (7c)$$

$$Q_i = \sum_{\beta=A,B} \left[Q_i^\beta - \frac{5}{2} X_0^\beta (u_i - u_i^\beta) \right]. \quad (7d)$$

If we denote by $X_0^\alpha + \chi^\alpha$ the concentration of species α , χ^α is expressed as

$$\chi^\alpha = N^\alpha - X_0^\alpha N. \quad (8)$$

Note that $\chi^A = -\chi^B$ because of the relations $N = N^A + N^B$ and $X_0^A + X_0^B = 1$.

Integrating Eq. (1) multiplied by E^α over the whole space of $\boldsymbol{\zeta}$ gives

$$\frac{d}{dx_1} \int \zeta_1 \phi^\alpha E^\alpha d^3\boldsymbol{\zeta} = 0. \quad (9a)$$

Similarly, integrating Eq. (1) multiplied by $\hat{m}^\alpha \zeta_i E^\alpha$ and that multiplied by $\hat{m}^\alpha \zeta_i^2 E^\alpha$ over the whole space of $\boldsymbol{\zeta}$ and taking the summation of the resulting equations for $\alpha=A, B$ give

$$\frac{d}{dx_1} \sum_{\alpha=A,B} \int \hat{m}^\alpha \zeta_1 \zeta_i \phi^\alpha E^\alpha d^3\boldsymbol{\zeta} = 0, \quad (9b)$$

$$\frac{d}{dx_1} \sum_{\alpha=A,B} \int \hat{m}^\alpha \zeta_1 \zeta_i^2 \phi^\alpha E^\alpha d^3\boldsymbol{\zeta} = 0. \quad (9c)$$

Equations (9a)–(9c) correspond to the conservation laws of the mass, momentum, and energy, respectively. Taking into account the condition at infinity, they are reduced to

$$u_1^\alpha = u_\infty, \quad (10a)$$

$$P_{11} = P_\infty, \quad P_{12} = P_{13} = 0, \quad (10b)$$

$$Q_1 = 0. \quad (10c)$$

III. PRELIMINARY ANALYSIS

A. Knudsen-layer problem

We will seek the solution of the boundary-value problem (1)–(5) in the form

$$\phi^\alpha = \phi_\infty^\alpha + \phi_K^\alpha(x_1, \zeta_i) u_\infty. \quad (11)$$

Substitution of Eq. (11) to Eqs. (1)–(5) gives the following equation and boundary condition for ϕ_K^α :

$$\zeta_1 \frac{\partial \phi_K^\alpha}{\partial x_1} = \sum_{\beta=A,B} K^{\beta\alpha} \tilde{L}^{\beta\alpha} (X_0^\alpha \phi_K^\beta, X_0^\beta \phi_K^\alpha), \quad (12)$$

$$\begin{aligned} \phi_K^\alpha &= X_0^\alpha \left[-\gamma^\alpha - \delta \left(\hat{m}^\alpha \zeta_i^2 - \frac{5}{2} \right) - 2\hat{m}^\alpha \zeta_1 \right], \\ \zeta_1 &> 0, \quad x_1 = 0, \end{aligned} \quad (13)$$

$$\phi_K^\alpha \rightarrow 0 \quad \text{as} \quad x_1 \rightarrow \infty, \quad (14)$$

where

$$\gamma^\alpha = \frac{P_\infty X_0^\alpha + \chi_\infty^\alpha}{u_\infty X_0^\alpha}, \quad (15a)$$

$$\delta = \frac{\tau_\infty}{u_\infty}. \quad (15b)$$

We call the half-space problem (12)–(14) the Knudsen-layer problem for evaporation and condensation. For the problem, there is a unique solution ϕ_K^α if and only if the constants γ^A , γ^B , and δ take special values, and ϕ_K^α decays exponentially as $x_1 \rightarrow \infty$. This is a consequence of the existence and uniqueness theorem for the Knudsen-layer problem for a binary mixture of hard-sphere gases (Ref. 32; see also Refs. 33–38 for the corresponding theorems for a single-component gas).

As is seen from Eq. (15), the fact that γ^A , γ^B , and δ take special values means that there are certain relations among the parameters P_∞ , χ_∞^A , τ_∞ , and u_∞ that characterize the state of the vapors at a far distance. To be more specific, the relations that hold among the parameters can be written as

$$P_\infty = \gamma u_\infty, \quad (16a)$$

$$\chi_\infty^A = (\gamma^A - \gamma^B) X_0^B X_0^A u_\infty, \quad (16b)$$

$$\tau_\infty = \delta u_\infty, \quad (16c)$$

or, equivalently,

$$p_\infty - p_0 = \gamma p_0 (2kT_0/m^A)^{-1/2} v_\infty, \quad (17a)$$

$$X_\infty^A - X_0^A = (\gamma^A - \gamma^B) X_0^B X_0^A (2kT_0/m^A)^{-1/2} v_\infty, \quad (17b)$$

$$T_\infty - T_0 = \delta T_0 (2kT_0/m^A)^{-1/2} v_\infty, \quad (17c)$$

where p_∞ , X_∞^A , T_∞ , and v_∞ are the pressure, concentration of species A , temperature, and flow velocity at a far distance, and

$$\gamma = \gamma^A X_0^A + \gamma^B X_0^B. \quad (18)$$

The set of relations (16a)–(16c) [or (17a)–(17c)] is a natural extension of the counterpart for a single-component vapor to a mixture of two species vapors. In the case of a single-component vapor, it is known^{5,6} that the state of the vapor at a far distance in this context can be regarded as that at the interface in the fluid-dynamic description. In other words, Eqs. (16a)–(16c) [or (17a)–(17c)] are regarded as the boundary condition for the fluid-dynamic equations at the interface. The same is true in the case of mixtures. Note that the relations (16a)–(16c) [or (17a)–(17c)] give the differences (the “jumps”) of those values that the pressure of the mixture, concentration of species A , and temperature of the mixture take at the surface of the condensed phase in the fluid-dynamic description from those specifying the state of the condensed phase. From this viewpoint, we call the relation (16a) [or (17a)] the jump condition for pressure, (16b) [or (17b)] that for concentration, and (16c) [or (17c)] that for temperature, respectively.

Since $\hat{m}^A = \hat{d}^A = 1$ and $X_0^A + X_0^B = 1$, the problem is characterized by the three parameters

$$\hat{m}^B \text{ (or } m^B/m^A), \quad \hat{d}^B \text{ (or } d^B/d^A), \quad X_0^A.$$

B. Similarity solution and macroscopic quantities

Thanks to the spherical symmetry⁶ of the collision operator $\tilde{L}^{\beta\alpha}$, we can seek the solution ϕ_K^α as a function of x_1 , ζ_1 , and ζ_ρ , where $\zeta_\rho = \sqrt{\zeta_2^2 + \zeta_3^2}$. By using the new notations

$$\Psi^\alpha(x_1, \zeta_1, \zeta_\rho) = \phi_K^\alpha(x_1, \zeta_1) E^\alpha, \quad (19a)$$

$$L^{\beta\alpha}(\Psi^\beta, \Psi^\alpha) = \tilde{L}^{\beta\alpha}(\phi_K^\beta, \phi_K^\alpha) E^\alpha, \quad (19b)$$

we rewrite Eqs. (12)–(14) as follows:

$$\zeta_1 \frac{\partial \Psi^\alpha}{\partial x_1} = \sum_{\beta=A,B} K^{\beta\alpha} L^{\beta\alpha}(X_0^\alpha \Psi^\beta, X_0^\beta \Psi^\alpha), \quad (20)$$

$$\Psi^\alpha = X_0^\alpha \left[-\gamma^\alpha - \delta \left(\hat{m}^\alpha (\zeta_1^2 + \zeta_\rho^2) - \frac{\zeta_1}{2} \right) - 2\hat{m}^\alpha \zeta_1 \right] E^\alpha, \quad (21)$$

$$\zeta_1 > 0, \quad x_1 = 0,$$

$$\Psi^\alpha \rightarrow 0 \quad \text{as } x_1 \rightarrow \infty. \quad (22)$$

Here E^α is regarded as a function of ζ_1 and ζ_ρ because $|\zeta| = (\zeta_1^2 + \zeta_\rho^2)^{1/2}$. The collision integral $L^{\beta\alpha}$ can be expressed in terms of integral kernels. The explicit form is given in Appendix A.

The macroscopic quantities defined by Eqs. (6)–(8) can be expressed by the moments of Ψ^α as follows:

$$N^\alpha = [X_0^\alpha (\gamma^\alpha - \delta) + \Omega^\alpha] u_\infty, \quad (23a)$$

$$u_1^\alpha = u_\infty, \quad (23b)$$

$$\chi^\alpha = [X_0^\alpha (\gamma^\alpha - \gamma) + \Omega^\alpha - X_0^\alpha \Omega] u_\infty, \quad (23c)$$

$$\tau^\alpha = (\delta + \Theta^\alpha) u_\infty, \quad (23d)$$

$$P^\alpha = (\gamma^\alpha X_0^\alpha + \Omega^\alpha + X_0^\alpha \Theta^\alpha) u_\infty, \quad (23e)$$

$$P_{11}^\alpha = (\gamma^\alpha X_0^\alpha + S_1^\alpha) u_\infty, \quad (23f)$$

$$P_{22}^\alpha = P_{33}^\alpha = (\gamma^\alpha X_0^\alpha + S_2^\alpha) u_\infty, \quad (23g)$$

$$Q_1^\alpha = H^\alpha u_\infty \quad (23h)$$

and

$$N = (\gamma - \delta + \Omega) u_\infty, \quad (24a)$$

$$u_1 = u_\infty, \quad (24b)$$

$$\tau = (\delta + \Theta) u_\infty, \quad (24c)$$

$$P = (\gamma + \Omega + \Theta) u_\infty, \quad (24d)$$

$$P_{11} = \gamma u_\infty, \quad (24e)$$

$$P_{22} = \left[\gamma + \frac{3}{2}(\Omega + \Theta) \right] u_{\infty}, \quad (24f)$$

$$Q_1 = 0, \quad (24g)$$

where

$$\Omega^{\alpha}(x_1) = 2\pi \int_0^{\infty} \int_{-\infty}^{\infty} \zeta_{\rho} \Psi^{\alpha} d\zeta_1 d\zeta_{\rho}, \quad (25a)$$

$$S_1^{\alpha}(x_1) = 4\pi \int_0^{\infty} \int_{-\infty}^{\infty} \hat{m}^{\alpha} \zeta_1^2 \zeta_{\rho} \Psi^{\alpha} d\zeta_1 d\zeta_{\rho}, \quad (25b)$$

$$S_2^{\alpha}(x_1) = 2\pi \int_0^{\infty} \int_{-\infty}^{\infty} \hat{m}^{\alpha} \zeta_{\rho}^3 \Psi^{\alpha} d\zeta_1 d\zeta_{\rho}, \quad (25c)$$

$$\Theta^{\alpha}(x_1) = \frac{1}{3X_0^{\alpha}} [S_1^{\alpha}(x_1) + 2S_2^{\alpha}(x_1) - 3\Omega^{\alpha}(x_1)], \quad (25d)$$

$$H^{\alpha}(x_1) = 2\pi \int_0^{\infty} \int_{-\infty}^{\infty} \hat{m}^{\alpha} \zeta_1 \zeta_{\rho} (\zeta_1^2 + \zeta_{\rho}^2) \Psi^{\alpha} d\zeta_1 d\zeta_{\rho} \quad (25e)$$

and

$$\Omega(x_1) = \Omega^A(x_1) + \Omega^B(x_1), \quad (26a)$$

$$\Theta(x_1) = X_0^A \Theta^A(x_1) + X_0^B \Theta^B(x_1). \quad (26b)$$

The other quantities in Eqs. (6)–(8) vanish because the integrands in their definitions are odd functions of ζ_2 or ζ_3 . In deriving the expressions above, the properties (9a)–(9c) [or Eqs. (10a)–(10c)] have been taken into account. It should be noted that the relations

$$S_1^A + S_1^B = 0, \quad H^A + H^B = 0 \quad (27)$$

hold because of Eqs. (7c) and (7d). The relations will be used as a measure of accuracy of the numerical solution (see Appendix B). In the sequel we will call the quantities defined by Eqs. (25) and (26) the Knudsen-layer functions.

IV. NUMERICAL ANALYSIS

Following Refs. 39 and 12–14, we solve the boundary-value problem (20)–(22) by the use of the following technique.

Consider the function $\tilde{\Psi}^{\alpha}$ and the constants γ_*^{α} and δ_* defined by

$$\tilde{\Psi}^{\alpha}(x_1, \zeta_1, \zeta_{\rho}) = \Psi^{\alpha}(x_1, \zeta_1, \zeta_{\rho}) + X_0^{\alpha} \left[\epsilon_1^{\alpha} + \epsilon_2 \left(\hat{m}^{\alpha} (\zeta_1^2 + \zeta_{\rho}^2) - \frac{5}{2} \right) \right] E^{\alpha}, \quad (28a)$$

$$\gamma_*^{\alpha} = \gamma^{\alpha} - \epsilon_1^{\alpha}, \quad \delta_* = \delta - \epsilon_2, \quad (28b)$$

where ϵ_1^{α} and ϵ_2 are undetermined constants. The function $\tilde{\Psi}^{\alpha}$ satisfies Eq. (20) and boundary condition (21) with γ^{α} and δ replaced by γ_*^{α} and δ_* , i.e.,

$$\zeta_1 \frac{\partial \tilde{\Psi}^{\alpha}}{\partial x_1} = \sum_{\beta=A,B} K^{\beta\alpha} L^{\beta\alpha} (X_0^{\alpha} \tilde{\Psi}^{\beta}, X_0^{\beta} \tilde{\Psi}^{\alpha}), \quad (29)$$

$$\tilde{\Psi}^{\alpha} = X_0^{\alpha} \left[-\gamma_*^{\alpha} - \delta_* \left(\hat{m}^{\alpha} (\zeta_1^2 + \zeta_{\rho}^2) - \frac{5}{2} \right) - 2\hat{m}^{\alpha} \zeta_1 \right] E^{\alpha}, \quad (30)$$

$$\zeta_1 > 0, \quad x_1 = 0.$$

At a large distance d for which Ψ^{α} is negligibly small, $\tilde{\Psi}^{\alpha}$ satisfies the reflection condition

$$\tilde{\Psi}^{\alpha}(d, \zeta_1, \zeta_{\rho}) = \tilde{\Psi}^{\alpha}(d, -\zeta_1, \zeta_{\rho}), \quad (31)$$

and ϵ_1^{α} and ϵ_2 are related to the following moments of $\tilde{\Psi}^{\alpha}$:

$$\epsilon_1^{\alpha} = \frac{\tilde{\Omega}^{\alpha}(d) + X_0^{\alpha} \tilde{\Theta}(d)}{X_0^{\alpha}}, \quad \epsilon_2 = \tilde{\Theta}(d), \quad (32)$$

where $\tilde{\Omega}^{\alpha}(x_1)$ and $\tilde{\Theta}(x_1)$ are the quantities defined by Eqs. (25a)–(25d) and (26b) with Ψ^{α} replaced by $\tilde{\Psi}^{\alpha}$. We solve the boundary-value problem (29)–(31) for given values of γ_*^{α} and δ_* under a proper choice of d . Once $\tilde{\Psi}^{\alpha}$ is obtained, ϵ_1^{α} and ϵ_2 are determined by Eq. (32). Then Ψ^{α} , γ^{α} , and δ are obtained by Eq. (28). In the actual computation, we repeat this solution process by putting γ^{α} and δ as new γ_*^{α} and δ_* in order to avoid the accumulation of the numerical errors caused by the computation of the collision integrals of the second term of Eq. (28a) in the wide region of x_1 space.

The numerical method is essentially the same as that in Refs. 12–14. To be more specific, with positive parameters d , Z_1 , and Z_{ρ} large enough, we limit x_1 , ζ_1 , and ζ_{ρ} spaces to finite regions given by $0 \leq x_1 \leq d$, $-Z_1 \leq \sqrt{\hat{m}^{\alpha}} \zeta_1 \leq Z_1$, and $0 \leq \sqrt{\hat{m}^{\alpha}} \zeta_{\rho} \leq Z_{\rho}$ for species α and use the same finite-difference scheme and the same lattice systems as those in Ref. 14. The finite regions are divided into N_x , $4N_1$, and $2N_{\rho}$ intervals as $0 = x_1^{(0)} < \dots < x_1^{(N_x)} = d$, $-Z_1 / \sqrt{\hat{m}^{\alpha}} = \zeta_1^{(-2N_1)} < \dots < \zeta_1^{(0)} (= 0) < \zeta_1^{(1)} < \dots < \zeta_1^{(2N_1)} = Z_1 / \sqrt{\hat{m}^{\alpha}}$, and $0 = \zeta_{\rho}^{(0)} < \dots < \zeta_{\rho}^{(2N_{\rho})} = Z_{\rho} / \sqrt{\hat{m}^{\alpha}}$ for species α (thus lattice points in the molecular space depend on species); the interval of lattice is uniform for ζ_{ρ} but nonuniform for x_1 and ζ_1 : smaller intervals for smaller x_1 and smaller $|\zeta_1|$. The only difference from Ref. 14 is the form of the collision integrals.

In the finite-difference scheme, the unknown function $\tilde{\Psi}^{\alpha}$ is solved iteratively. The collision integrals $L^{\beta\alpha}(X_0^{\alpha} \tilde{\Psi}^{\beta}, X_0^{\beta} \tilde{\Psi}^{\alpha})$ at the lattice point $(x_1^{(i)}, \zeta_1^{(j)}, \zeta_{\rho}^{(k)})$ at the n th step of iteration are computed as

$$\begin{aligned} & L^{\beta\alpha}(X_0^{\alpha} \tilde{\Psi}^{\beta}, X_0^{\beta} \tilde{\Psi}^{\alpha})(x_1^{(i)}, \zeta_1^{(j)}, \zeta_{\rho}^{(k)}) \\ &= \sum_{l=-2N_1}^{2N_1} \sum_{m=0}^{2N_{\rho}} [M_{1(j,k,l,m)}^{\beta\alpha} \tilde{\Psi}^{\beta(n-1)}(x_1^{(i)}, \zeta_1^{(l)}, \zeta_{\rho}^{(m)}) \\ & \quad + M_{2(j,k,l,m)}^{\beta\alpha} \tilde{\Psi}^{\alpha(n-1)}(x_1^{(i)}, \zeta_1^{(l)}, \zeta_{\rho}^{(m)})] \\ & \quad - X_0^{\beta} \nu^{\beta}(\zeta_1^{(j)}, \zeta_{\rho}^{(k)}) \tilde{\Psi}^{\alpha(n)}(x_1^{(i)}, \zeta_1^{(j)}, \zeta_{\rho}^{(k)}), \end{aligned} \quad (33)$$

where $\tilde{\Psi}^{\alpha(n)}$ denotes $\tilde{\Psi}^{\alpha}$ at the n th step of iteration, and ν^{β} is a given function defined by Eq. (A2b). Here ν^{β} is regarded as a function of ζ_1 and ζ_{ρ} since $|\zeta| = (\zeta_1^2 + \zeta_{\rho}^2)^{1/2}$. The $M_{1(j,k,l,m)}^{\beta\alpha}$ and $M_{2(j,k,l,m)}^{\beta\alpha}$ are universal matrices, which we call the *numerical kernel*; they are independent of the step of iteration and the unknown functions $\tilde{\Psi}^{\alpha}$ and $\tilde{\Psi}^{\beta}$ and thus can be prepared before the iteration solution process. Since the colli-

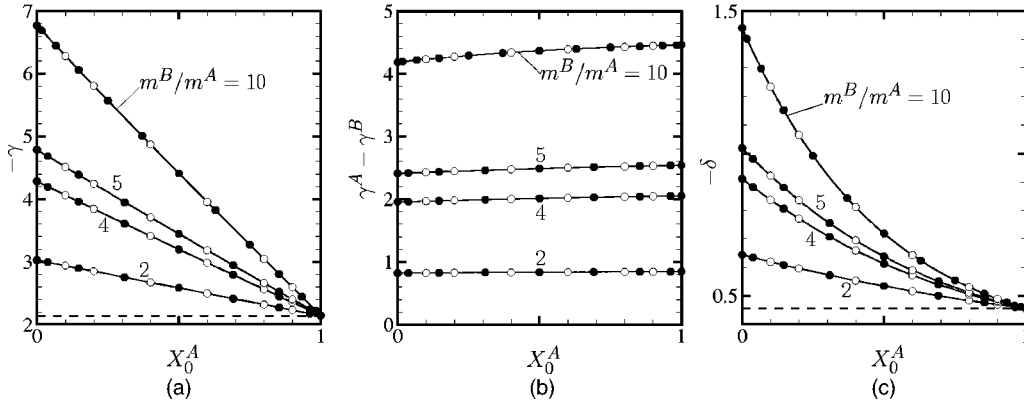


FIG. 1. Coefficients in the jump condition (17). (a) γ vs X_0^A , (b) $\gamma^A - \gamma^B$ vs X_0^A , and (c) δ vs X_0^A . Both closed and open circles indicate the present result. The solid line indicates the present result using the formula (34). The data used to construct the formula are marked with closed circles. The dashed line indicates the result for $m^B/m^A=1$.

sion integrals are different from those in Ref. 14, we newly construct and store the data of the numerical kernel in the present work. Several tests are performed to assess the accuracy of the computation of the collision integrals. The results are summarized in Appendix B.

After a series of accuracy tests parallel to those performed in Refs. 13 and 14, we adopt $(S1, M1)$ and $(S4, M1)$ in Ref. 14 as the standard lattice system; the former is used for $m^B/m^A=2$ and the latter is used for $m^B/m^A=4, 5, 10$. Here $S1$ and $S4$ are the lattice systems for x_1 space. For the former, the computation region is limited to $0 \leq x_1 \leq 24.08$ ($d=24.08$) and there are 301 lattice points ($N_x=300$). For the latter, the region is $0 \leq x_1 \leq 32.49$ ($d=32.49$) and there are 341 lattice points ($N_x=340$). $M1$ is the lattice system for ζ_1 and ζ_ρ spaces. The computation regions are limited to $-4.5 \leq \sqrt{\hat{m}^\alpha} \zeta_1 \leq 4.5$ and $0 \leq \sqrt{\hat{m}^\alpha} \zeta_\rho \leq 4.5$ for species α ($Z_1=Z_\rho=4.5$), and there are 101 and 55 lattice points, respectively ($N_1=25$ and $N_\rho=27$). (See Refs. 13 and 14 for the complete information about the lattice system.) The results of the accuracy tests are summarized in Appendix B. The results shown in the following section are obtained by the use of the standard lattice systems.

The computation was mainly performed by using a parallel code for ten CPUs on the FUJITSU VPP800 in the Academic Center for Computing and Media Studies of Kyoto University. First the computation was carried out for a smaller lattice system with $301 \times 73 \times 21$ points in $(x_1, \zeta_1, \zeta_\rho)$ -space [system $(S1, M7)$], and the resulting data were transformed into the data for the standard lattice system by interpolation and extrapolation. Then, the computation for the standard system $(S1, M1)$ or $(S4, M1)$ was performed by using the transformed data as the initial guess in the iterative solution process. For each set of parameters $(m^B/m^A, d^B/d^A, X_0^A)$, it takes about half an hour for the smaller system, 3 h for system $(S1, M1)$, and 3.5 h for system $(S4, M1)$. The computing time does not depend much on the values of the parameters. Auxiliary computations were carried out on the FUJITSU VPP800 in the Center for Planning and Information Systems of the Japan Aerospace Exploration Agency.

V. RESULTS AND DISCUSSIONS

In the present paper, we carry out the computation for $m^B/m^A=2, 4, 5, 10$ and for various values of X_0^A , restricting ourselves to the case $d^B/d^A=1$. Hereinafter, we assume that $m^B/m^A \geq 1$, because the results for $m^B/m^A < 1$ can be obtained from those for $m^B/m^A > 1$ by a simple transformation.

A. Coefficients in the jump condition

The coefficients γ , $\gamma^A - \gamma^B$, and δ in the jump condition (17) versus the concentration X_0^A of species A are shown in Fig. 1. Since γ is negative, the pressure of the mixture at a far distance is lower (higher) than that of the saturated mixture of vapors if the evaporation (condensation) takes place [see Eq. (17a)]. The same is true for the temperature of the mixture because δ is also negative. On the contrary, since $\gamma^A - \gamma^B$ is positive, the concentration of the species with smaller molecular mass (species A in the present parameter settings) at a far distance is higher (lower) than that of the saturated mixture if the evaporation (condensation) takes place. The coefficients are independent of X_0^A for $m^B/m^A=1$ because there is no difference between molecules of different kinds. They are, however, not uniform for $m^B/m^A \neq 1$ and become monotonically increasing or decreasing functions of X_0^A . It should be noted that the values of γ and δ at $X_0^A=0$ (the case of pure gas B) are the same as those at $X_0^A=1$ (the case of pure gas A) multiplied by $\sqrt{m^B/m^A}$. This is easily seen by a simple transformation of the reference velocity.

The numerical computations are performed for several values of X_0^A , the results of which are indicated by closed or open circles in Fig. 1. From the data shown by closed circles, following Ref. 13, we constructed the formulas of γ^A , γ^B , and δ for arbitrary values of X_0^A by the use of the Chebyshev polynomial approximation (Ref. 40). The formulas are written as

TABLE I. Data of $\gamma^{A(n)}$ ($n=0, \dots, N$) in Eq. (34).

n	m^B/m^A			
	2 ($N=8$)	4 ($N=8$)	5 ($N=8$)	10 ($N=12$)
0	-2.169 57	-2.212 35	-2.229 51	-2.294 26
1	3.272 90(-2) ^a	8.992 91(-2)	1.141 49(-1)	2.090 38(-1)
2	-4.571 78(-3)	-2.106 28(-2)	-2.947 27(-2)	-6.718 39(-2)
3	2.908 33(-4)	2.451 73(-3)	3.938 65(-3)	1.288 72(-2)
4	-2.037 58(-7)	-6.921 72(-5)	-1.923 33(-4)	-1.754 17(-3)
5	-1.939 31(-6)	-3.199 94(-5)	-4.275 62(-5)	1.501 21(-4)
6	1.738 91(-7)	6.059 70(-6)	1.076 90(-5)	-2.670 55(-6)
7	5.165 64(-10)	-1.767 19(-7)	-6.060 30(-7)	-8.501 90(-7)
8	-1.639 32(-9)	-1.150 97(-7)	-1.994 79(-7)	-1.518 00(-7)
9	1.191 74(-7)
10	-3.244 54(-8)
11	5.638 43(-9)
12	-8.125 55(-11)

^aRead as $3.272\ 90 \times 10^{-2}$.

$$h = \sum_{n=0}^N h^{(n)} T_n(2X_0^A - 1), \quad (34)$$

with $h = \gamma^A$, γ^B , and δ , where $T_n(x)$ ($n=0, 1, 2, \dots$) is the Chebyshev polynomial of degree n defined for $0 \leq \theta \leq \pi$ by the relation

$$T_n(\cos \theta) = \cos n\theta. \quad (35)$$

The data of $\gamma^{A(n)}$, $\gamma^{B(n)}$, and $\delta^{(n)}$ are listed in Tables I–III. The solid line in Fig. 1 is drawn by using Eq. (34). The accuracy of this formula is checked by comparing with the data shown by open circles in the figure. The results are summarized at the end of Appendix B. Some of the values of γ , $\gamma^A - \gamma^B$, and δ obtained by Eq. (34) are shown in Table IV.

In the case of gas mixtures, compared to the jump phenomenon caused by the gradients of temperature and concentration, much less attention has been paid to the present problem. This is probably due to that a mixture of

noncondensable gases instead of that of vapors was mainly treated in the literature.²⁷ The available data are limited. Here we make a comparison, in Table V, with the data in Refs. 25 and 26.⁴¹ Their data are obtained by an approximation method that they call the *modification of Maxwell's method* or the *Maxwell–Loyalka method*. Their method is based on an arbitrary assumption. Nevertheless both results agree with the present one within 3% for the coefficients γ , $\gamma^A - \gamma^B$, and δ . On the contrary, the agreement is poorer if one observes the coefficients γ^A and γ^B separately. The data of γ^A in Ref. 25 differs from the present one by about 8% at worst. Incidentally, the formulas of γ in Refs. 25 and 26 are common to each other.

As is stressed in the Introduction, the linearized problem itself has a physical significance, independent of the nonlinear problem. Nevertheless one may still have an interest in the range of “validity” of the solution of the linearized problem when regarded as an approximation for the nonlinear

TABLE II. Data of $\gamma^{B(n)}$ ($n=0, \dots, N$) in Eq. (34).

n	m^B/m^A			
	2 ($N=8$)	4 ($N=8$)	5 ($N=8$)	10 ($N=12$)
0	-3.002 35	-4.221 32	-4.712 49	-6.638 85
1	2.135 60(-2) ^a	4.202 06(-2)	4.912 84(-2)	7.508 82(-2)
2	-3.983 24(-3)	-1.622 20(-2)	-2.189 57(-2)	-4.496 30(-2)
3	3.134 06(-4)	2.494 54(-3)	3.813 69(-3)	1.002 26(-2)
4	-8.255 13(-6)	-1.985 29(-4)	-3.802 38(-4)	-1.678 59(-3)
5	-1.211 69(-6)	-7.711 30(-6)	6.031 01(-7)	2.032 04(-4)
6	1.612 22(-7)	4.473 15(-6)	6.824 65(-6)	-1.572 12(-5)
7	-4.002 06(-9)	-4.393 04(-7)	-9.504 70(-7)	4.867 96(-7)
8	-1.112 97(-9)	-3.668 51(-8)	-4.137 92(-8)	-6.612 65(-8)
9	6.195 92(-8)
10	-2.215 63(-8)
11	5.026 48(-9)
12	-2.024 69(-10)

^aRead as $2.135\ 60 \times 10^{-2}$.

TABLE III. Data of $\delta^{(n)}$ ($n=0, \dots, N$) in Eq. (34).

n	m^B/m^A			
	2 ($N=8$)	4 ($N=8$)	5 ($N=8$)	10 ($N=12$)
0	-5.423 40(-1) ^a	-6.485 14(-1)	-6.880 32(-1)	-8.317 95(-1)
1	9.412 08(-2)	2.251 63(-1)	2.769 64(-1)	4.738 93(-1)
2	-7.630 13(-3)	-3.501 37(-2)	-4.920 37(-2)	-1.142 98(-1)
3	2.384 17(-4)	2.696 31(-3)	4.703 25(-3)	1.855 08(-2)
4	2.503 36(-5)	1.386 91(-4)	6.520 90(-5)	-2.057 33(-3)
5	-3.579 18(-6)	-6.593 03(-5)	-9.838 94(-5)	1.114 54(-4)
6	9.504 55(-8)	6.373 86(-6)	1.315 56(-5)	7.317 05(-6)
7	2.543 76(-8)	6.754 26(-7)	6.380 40(-7)	-9.832 02(-7)
8	-3.700 56(-9)	-2.811 32(-7)	-5.162 62(-7)	-5.328 45(-7)
9	2.241 87(-7)
10	-4.707 31(-8)
11	6.218 38(-9)
12	1.185 42(-10)

^aRead as $-5.423\ 40 \times 10^{-1}$.

problem. Figure 2 shows a comparison with the results of the nonlinear problem taken from Ref. 42 in the case of evaporation, where numerical simulation is carried out by the direct simulation Monte Carlo method. In the figure, p_∞/p_0 , T_∞/T_0 , and X_∞^A are plotted as a function of the flow velocity v_∞ [see Eq. (17)]. The smooth transition of the results in Ref.

42 to the present results as v_∞ decreases is observed. In the case of condensation, the nonlinear problem concludes a jump condition of different form from Eq. (17), however small the flow Mach number might be. (See the second paragraph from the end of the Introduction. There is a qualitative difference of the condition between the evaporation and con-

TABLE IV. The values of γ , $\gamma^A - \gamma^B$, and δ by the formula (34).

$X_0^A m^B/m^A$	$-\gamma$			
	2	4	5	10
0	3.0280	4.2822	4.7877	6.7708
0.1	2.9381	4.0615	4.5134	6.2831
0.3	2.7593	3.6268	3.9749	5.3362
0.5	2.5817	3.1983	3.4456	4.4122
0.7	2.4050	2.7738	2.9217	3.5000
0.9	2.2289	2.3517	2.4009	2.5935
1	2.1411	2.1411	2.1411	2.1411
$X_0^A m^B/m^A$	$\gamma^A - \gamma^B$			
	2	4	5	10
0	0.8208	1.9564	2.4105	4.1856
0.1	0.8235	1.9691	2.4287	4.2322
0.3	0.8286	1.9931	2.4623	4.3089
0.5	0.8334	2.0139	2.4907	4.3667
0.7	0.8377	2.0314	2.5140	4.4106
0.9	0.8417	2.0459	2.5327	4.4446
1	0.8435	2.0521	2.5407	4.4591
$X_0^A m^B/m^A$	$-\delta$			
	2	4	5	10
0	0.6443	0.9112	1.0187	1.4407
0.1	0.6197	0.8377	0.9219	1.2345
0.3	0.5746	0.7122	0.7608	0.9261
0.5	0.5347	0.6134	0.6388	0.7196
0.7	0.4997	0.5372	0.5483	0.5818
0.9	0.4693	0.4792	0.4819	0.4896
1	0.4556	0.4556	0.4556	0.4556

TABLE V. A comparison with the previous results of the coefficients γ , $\gamma^A - \gamma^B$, and δ in the jump condition (17).

		$X_0^A=0.1$							
		$-\gamma$		$\gamma^A - \gamma^B$			$-\delta$		
m^B/m^A		Present result	Refs. 25 and 26	Present result	Ref. 25	Ref. 26	Present result	Ref. 25	Ref. 26
2		2.9381	2.9161	0.8235	0.8345	0.8192	0.6197	0.6085	0.6085
4		4.0615	4.0292	1.9691	2.0146	1.9437	0.8377	0.8226	0.8226
5		4.5134	4.4762	2.4287	2.4902	2.3989	0.9219	0.9050	0.9051
10		6.2831	6.2232	4.2322	4.3561	4.1863	1.2345	1.2081	1.2084
		$X_0^A=0.5$							
		$-\gamma$		$\gamma^A - \gamma^B$			$-\delta$		
m^B/m^A		Present result	Refs. 25 and 26	Present result	Ref. 25	Ref. 26	Present result	Ref. 25	Ref. 26
2		2.5817	2.5616	0.8334	0.8345	0.8130	0.5347	0.5253	0.5253
4		3.1983	3.1696	2.0139	2.0146	1.9753	0.6134	0.6038	0.6040
5		3.4456	3.4128	2.4907	2.4902	2.4417	0.6388	0.6293	0.6295
10		4.4122	4.3610	4.3667	4.3561	4.2732	0.7196	0.7099	0.7106
		$X_0^A=0.9$							
		$-\gamma$		$\gamma^A - \gamma^B$			$-\delta$		
m^B/m^A		Present result	Refs. 25 and 26	Present result	Ref. 25	Ref. 26	Present result	Ref. 25	Ref. 26
2		2.2289	2.2122	0.8417	0.8345	0.8246	0.4693	0.4608	0.4608
4		2.3517	2.3327	2.0459	2.0146	1.9999	0.4792	0.4707	0.4707
5		2.4009	2.3809	2.5327	2.4902	2.4744	0.4819	0.4733	0.4733
10		2.5935	2.5691	4.4446	4.3561	4.3362	0.4896	0.4809	0.4810

densation cases.) In this sense, the comparison would be meaningless and is not made here. Incidentally, the qualitative difference of the jump condition between the evaporation and condensation was studied recently in Ref. 24 in the case of a binary mixture of vapors by an asymptotic analysis of the nonlinear problem for small Mach numbers.

B. Knudsen-layer functions and velocity distribution functions

The Knudsen-layer functions Ω^A/X_0^A , Ω^B/X_0^B , Θ^A , and Θ^B are shown in Figs. 3 and 4 and in Tables VI and VII. They decay rapidly to zero as the distance from the wall increases (the variations are not always monotonic). Their dependence on X_0^A is larger for larger m^B/m^A . The functions Ω^A/X_0^A and Θ^A (or Ω^B/X_0^B and Θ^B) do not vanish at $X_0^A=0$ (or $X_0^A=1$) because they are the quantities normalized by the reference concentration. The Knudsen-layer functions Ω and Θ for the mixture, which are linear combinations of the functions above, are shown in Fig. 5. Corresponding to the relation between (δ, γ) at $X_0^A=0$ and that at $X_0^A=1$ (see the first paragraph in Sec. V A), the profiles for $X_0^A=0$ are the same as those for $X_0^A=1$ multiplied by $\sqrt{m^B/m^A}$. The functions Ω and Θ at $X_0^A=1$, which can be considered as the corresponding functions for a single-species vapor, are shown in Table VIII. They have already been obtained in Ref. 39 by the same numerical method, i.e., the combination of the finite-difference and the numerical kernel methods. In the present

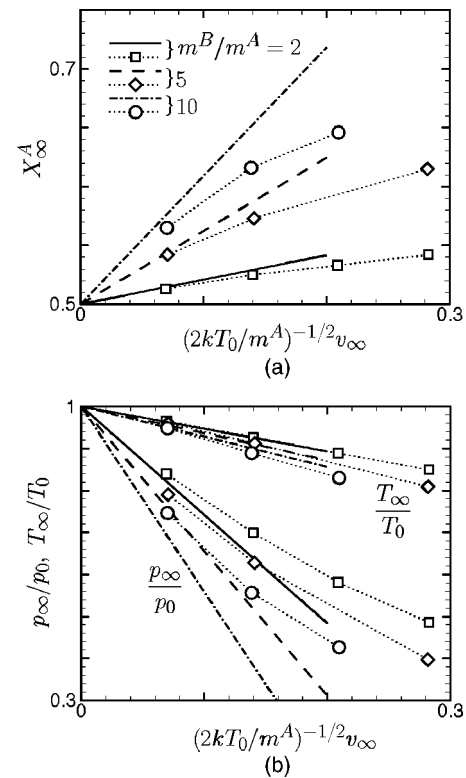


FIG. 2. Comparison of the jump condition (17) with the counterpart of the nonlinear problem in the case of evaporation ($X_0^A=0.5$). (a) X_∞^A vs $(2kT_0/m^A)^{-1/2}v_\infty$, (b) p_∞/p_0 and T_∞/T_0 vs $(2kT_0/m^A)^{-1/2}v_\infty$. The solid, dashed, and dot-dashed lines indicate the present results (linear problem), while the symbols \square , \diamond , and \circ connected with a dotted line the results in Ref. 42 (nonlinear problem). The mass ratio is shown in the figure.

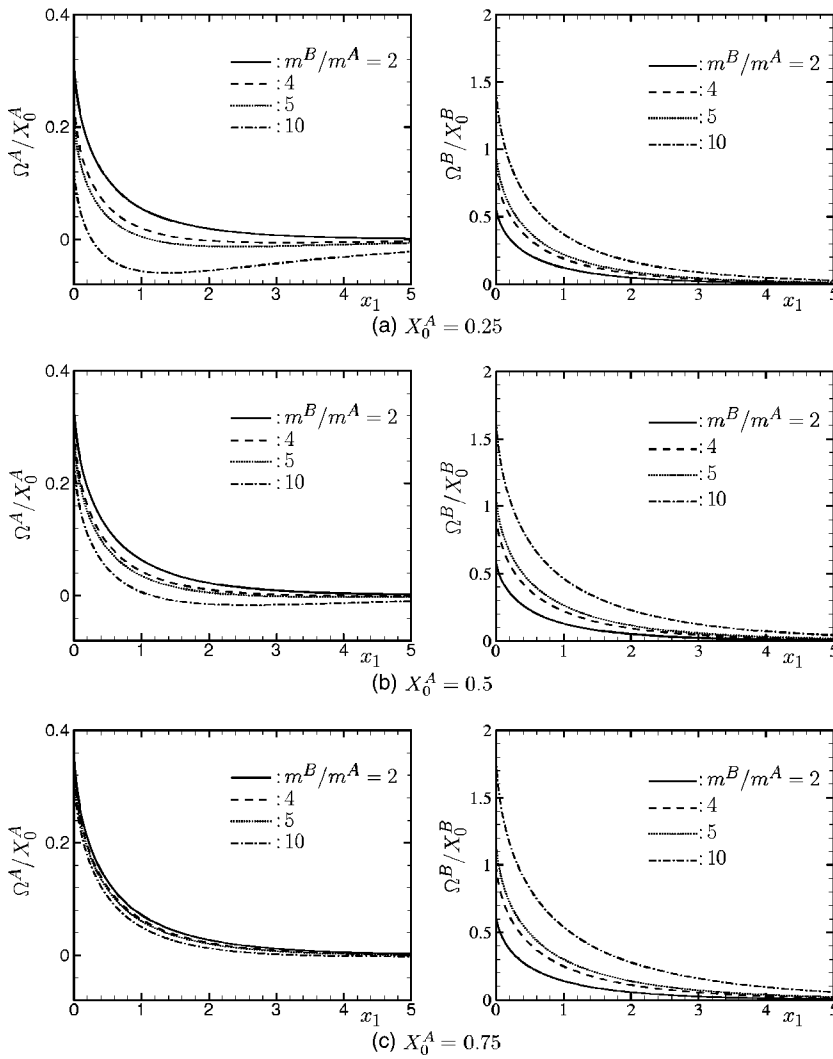


FIG. 3. Knudsen-layer functions Ω^A/X_0^A and Ω^B/X_0^B . (a) $X_0^A=0.25$, (b) $X_0^A=0.5$, and (c) $X_0^A=0.75$.

work, they are obtained with a higher accuracy. The difference is, at most, 7.7×10^{-5} for Ω and 2.7×10^{-5} for Θ . The Knudsen-layer functions S_1^A and H^A are also shown in Fig. 6 and Table IX. The functions S_1^B and H^B are readily obtained from the figure and the table by the relation (27). Note that S_1^A , S_1^B , H^A , and H^B all vanish at $X_0^A=0$ and 1.

The results for $X_0^A=0.25$ and 0.75 in the figures and tables in this section are obtained by the use of Chebyshev polynomial approximation from the data of Ω^A/X_0^A , Ω^B/X_0^B , Θ^A , Θ^B , S_1^A/X_0^A , S_1^B/X_0^B , H^A/X_0^A , and H^B/X_0^B at the values of X_0^A indicated by closed circles in Fig. 1. The FORTRAN code generating the Knudsen-layer functions for an arbitrary value of X_0^A is available from the authors.

The reduced velocity distribution functions Ψ^A and Ψ^B and their contour plots in the case of $m^B/m^A=5$ and $X_0^A=0.5$ are shown in Figs. 7 and 8. There is a discontinuity at $\zeta_1=0$ on the wall ($x_1=0$) [see Figs. 7(a) and 8(a)]. The discontinuity disappears immediately inside the gas,⁴³ but its trace remains as a steep gradient around $\zeta_1=0$ near the wall [see Figs. 7(b) and 8(b)]. As the distance from the wall increases, Ψ^α decays to zero with keeping the distinct difference in the shape between the positive and the negative regions of ζ_1 [see the transition of the contour plots from Fig. 7(a) to Fig. 7(d) and from Fig. 8(a) to Fig. 8(d)].

In Fig. 7(a), the distribution of outgoing molecules of species A from the condensed phase ($\zeta_1 > 0$) is rather flat in ζ_ρ for small $|\zeta|$. This feature is not always true. Figure 9 shows, as an example, the function Ψ^A at $x_1=0$ for different values of X_0^A for $m^B/m^A=5$. The variation of the function in ζ_ρ for small $|\zeta|$ depends much on X_0^A . This is a reflection of the dependence of magnitude of δ relative to $-\gamma^A + \frac{5}{2}\delta$ on X_0^A because the velocity distribution of outgoing molecules is given by Eq. (21) with $\alpha=A$. When $X_0^A=0.9$, $-\delta$ is about half of $-\gamma^A + \frac{5}{2}\delta$, so that the term of ζ_ρ^2 in the parentheses in Eq. (21) is not appreciable in the figure. On the other hand, when $X_0^A=0.5$ and 0.1, $-\delta$ is comparable or much superior to $-\gamma^A + \frac{5}{2}\delta$, and the term of ζ_ρ^2 becomes significant and its feature is readily seen in the figure. For species B, according to the numerical results, $-\delta$ is always smaller than half of $-\gamma^B + \frac{5}{2}\delta$, and thus the feature of the term $\hat{m}^B \zeta_\rho^2$ is not appreciable in the figure. The distribution of outgoing molecules of species B is always similar to that in Fig. 8(a) in its shape. Incidentally, the Ψ^A/X_0^A for $X_0^A=0.1$ and 0.9 in Fig. 9 is the one obtained by the use of Chebyshev polynomial approximation from its data at the values of X_0^A indicated by closed circles in Fig. 1.

TABLE VII. Knudsen-layer functions Ω^A/X_0^A , Ω^B/X_0^B , Θ^A , and Θ^B in the case of $m^B/m^A=5$.

$x_1 \setminus X_0^A$	Ω^A/X_0^A			Ω^B/X_0^B			Θ^A			Θ^B		
	0.25	0.5	0.75	0.25	0.5	0.75	0.25	0.5	0.75	0.25	0.5	0.75
0.0000	0.2166	0.2832	0.3365	0.9696	1.0789	1.1681	0.2728	0.1678	0.0975	-0.0157	-0.1137	-0.1810
0.0271	0.1818	0.2448	0.2950	0.8578	0.9558	1.0348	0.2572	0.1567	0.0901	-0.0140	-0.1019	-0.1604
0.0988	0.1358	0.1936	0.2394	0.7108	0.7966	0.8654	0.2324	0.1396	0.0786	-0.0133	-0.0880	-0.1356
0.2011	0.0975	0.1501	0.1917	0.5845	0.6605	0.7216	0.2076	0.1229	0.0677	-0.0134	-0.0765	-0.1152
0.3838	0.0573	0.1031	0.1394	0.4436	0.5086	0.5611	0.1757	0.1019	0.0542	-0.0139	-0.0638	-0.0930
0.5833	0.0319	0.0719	0.1037	0.3451	0.4015	0.4474	0.1499	0.0855	0.0440	-0.0141	-0.0545	-0.0774
0.7967	0.0152	0.0502	0.0780	0.2721	0.3213	0.3617	0.1284	0.0722	0.0360	-0.0140	-0.0472	-0.0654
1.1424	-0.0001	0.0285	0.0513	0.1928	0.2329	0.2663	0.1019	0.0562	0.0267	-0.0134	-0.0383	-0.0517
1.6669	-0.0097	0.0115	0.0287	0.1209	0.1509	0.1763	0.0737	0.0397	0.0177	-0.0118	-0.0288	-0.0378
2.4139	-0.0126	0.0015	0.0133	0.0666	0.0868	0.1044	0.0481	0.0253	0.0103	-0.0092	-0.0198	-0.0253
3.3368	-0.0108	-0.0021	0.0053	0.0340	0.0467	0.0579	0.0292	0.0151	0.0056	-0.0064	-0.0126	-0.0160
4.7525	-0.0067	-0.0025	0.0013	0.0132	0.0194	0.0252	0.0141	0.0072	0.0024	-0.0034	-0.0064	-0.0081
7.6134	-0.0020	-0.0010	0.0000	0.0023	0.0039	0.0054	0.0035	0.0018	0.0005	-0.0009	-0.0016	-0.0021
11.4643	-0.0004	-0.0002	0.0000	0.0003	0.0005	0.0008	0.0006	0.0003	0.0001	-0.0001	-0.0003	-0.0004
15.3020	-0.0001	0.0000	0.0000	0.0000	0.0001	0.0001	0.0001	0.0001	0.0000	0.0000	0.0000	-0.0001

VI. CONCLUDING REMARKS

In the present paper, we have investigated the half-space problem of evaporation and condensation for a binary mixture of vapors on the basis of the linearized Boltzmann equation.

The hard-sphere molecular model, which is the most fundamental model in kinetic theory, is adopted, and an accurate numerical solution is established at the level of the velocity distribution function as well as the macroscopic

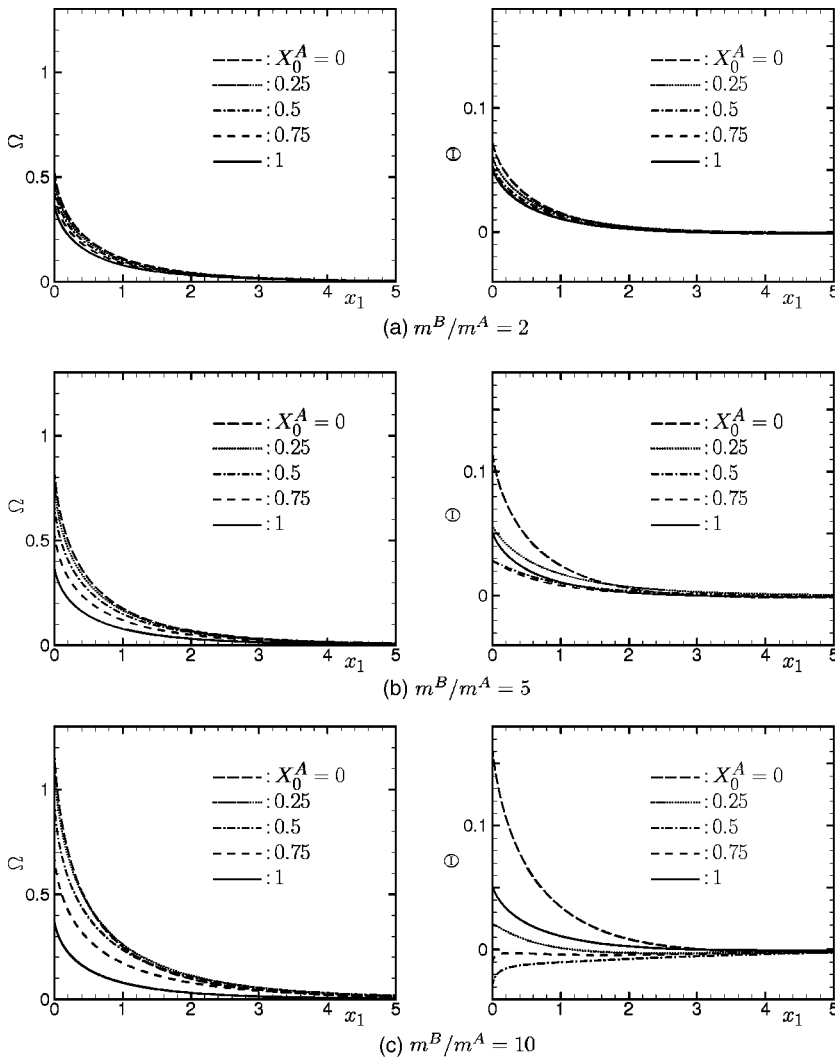


FIG. 5. Knudsen-layer functions Ω and Θ . (a) $m^B/m^A=2$, (b) $m^B/m^A=5$, and (c) $m^B/m^A=10$.

TABLE VIII. Knudsen-layer functions Ω and Θ for $X_0^A=1$, i.e., for a single-species vapor.

x_1	Ω	Θ
0.0000	0.3782	0.0520
0.0271	0.3338	0.0475
0.0988	0.2745	0.0404
0.2011	0.2234	0.0336
0.3838	0.1667	0.0252
0.5833	0.1275	0.0191
0.7967	0.0988	0.0143
1.1424	0.0683	0.0091
1.6669	0.0415	0.0045
2.4139	0.0220	0.0013
3.3368	0.0109	-0.0002
4.7525	0.0041	-0.0007
7.6134	0.0008	-0.0004
11.4643	0.0001	-0.0001
15.3020	0.0000	0.0000

quantities. The obtained jump coefficients would serve as the standard to assess the validity of approximate solution methods aiming at practical purposes.

In the case of a single-species vapor, according to Refs. 9 and 10, when the evaporation and condensation take place rather weakly, the vapor flow under the ordinary pressure can be described by the Navier–Stokes (or Stokes) equations equipped with the nonslip tangential velocity and the counterpart of the jump condition (17) as the boundary condition on the surface of the condensed phase. This is concluded by a systematic asymptotic analysis of the Boltzmann equation. It is possible by the parallel analysis to show that the same is true in the case of a mixture of vapors. That is, the Navier–Stokes (or Stokes) equations for gas mixtures equipped with the condition (17) and the nonslip tangential velocity at the surface of the condensed phase can describe the behavior of the vapors with the phase change at the surface under the ordinary pressure; consequently they would have a large potential application field, typically in chemical engineering processes such as distillation.

Further, recently, one of the authors demonstrated in the simple two-surface problem that the analysis of the present problem, together with the jump problems related to the temperature and concentration gradients, is inevitable to understand a certain singular behavior of a mixture of two species

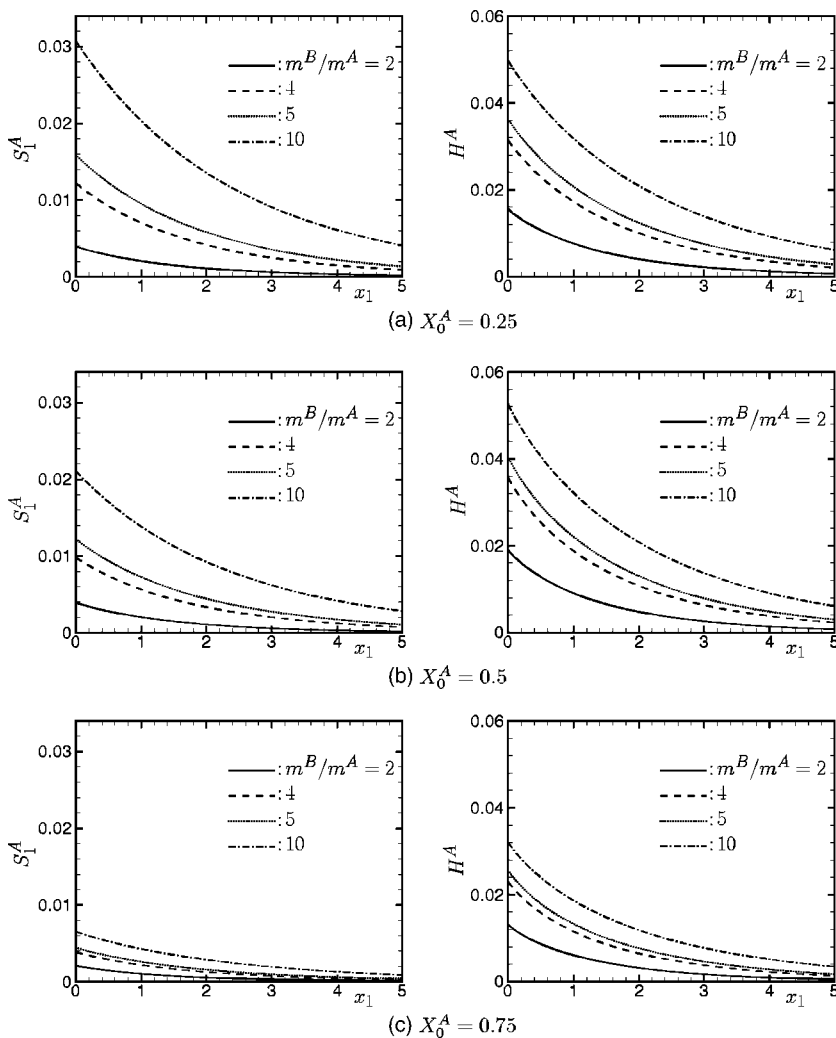


FIG. 6. Knudsen-layer functions S_1^A and H^A . (a) $X_0^A=0.25$, (b) $X_0^A=0.5$, and (c) $X_0^A=0.75$.

TABLE IX. Knudsen-layer functions S_1^A and H^A .

$x_1 \setminus X_0^A$	S_1^A						H^A					
	$m^B/m^A=2$			$m^B/m^A=5$			$m^B/m^A=2$			$m^B/m^A=5$		
	0.25	0.5	0.75	0.25	0.5	0.75	0.25	0.5	0.75	0.25	0.5	0.75
0.0000	0.0039	0.0039	0.0021	0.0159	0.0122	0.0044	0.0155	0.0190	0.0131	0.0363	0.0404	0.0256
0.0271	0.0039	0.0038	0.0020	0.0157	0.0120	0.0044	0.0152	0.0185	0.0127	0.0357	0.0396	0.0250
0.0988	0.0037	0.0036	0.0019	0.0151	0.0116	0.0042	0.0143	0.0174	0.0119	0.0341	0.0376	0.0236
0.2011	0.0034	0.0034	0.0018	0.0143	0.0109	0.0040	0.0132	0.0160	0.0109	0.0321	0.0351	0.0219
0.3838	0.0031	0.0030	0.0016	0.0130	0.0099	0.0036	0.0116	0.0139	0.0094	0.0289	0.0314	0.0193
0.5833	0.0027	0.0026	0.0014	0.0117	0.0090	0.0032	0.0101	0.0121	0.0081	0.0259	0.0279	0.0170
0.7967	0.0023	0.0023	0.0012	0.0105	0.0080	0.0029	0.0087	0.0104	0.0070	0.0231	0.0247	0.0149
1.1424	0.0019	0.0018	0.0010	0.0089	0.0067	0.0024	0.0070	0.0083	0.0055	0.0192	0.0204	0.0122
1.6669	0.0013	0.0013	0.0007	0.0068	0.0052	0.0019	0.0050	0.0059	0.0039	0.0147	0.0155	0.0092
2.4139	0.0008	0.0008	0.0004	0.0047	0.0036	0.0013	0.0031	0.0037	0.0024	0.0101	0.0106	0.0062
3.3368	0.0005	0.0005	0.0002	0.0030	0.0023	0.0008	0.0018	0.0021	0.0014	0.0064	0.0067	0.0039
4.7525	0.0002	0.0002	0.0001	0.0015	0.0012	0.0004	0.0008	0.0009	0.0006	0.0032	0.0034	0.0019
7.6134	0.0000	0.0000	0.0000	0.0004	0.0003	0.0001	0.0001	0.0002	0.0001	0.0008	0.0009	0.0005
11.4643	0.0000	0.0000	0.0000	0.0001	0.0001	0.0000	0.0000	0.0000	0.0000	0.0001	0.0001	0.0001
15.3020	0.0000	0.0000	0.0000	0.0000	0.0000	0.0000	0.0000	0.0000	0.0000	0.0000	0.0000	0.0000

vapors in the continuum limit.⁴⁴ There, the source of the singular behavior was clarified as a new category of the ghost effect^{6,45-47} that some of the gas rarefaction effects remain finite in the continuum limit. This gives a new significant role to the linearized jump problems for the understanding of the behavior of continuum gas flows with the phase transition.

ACKNOWLEDGMENTS

The present work was supported by the Grants-in-Aid for Scientific Research (Grant Nos. 14350047 and 15760108) from the Japan Society for the Promotion of Science and by the Center of Excellence for Research and Education on Complex Functional Mechanical Systems (COE

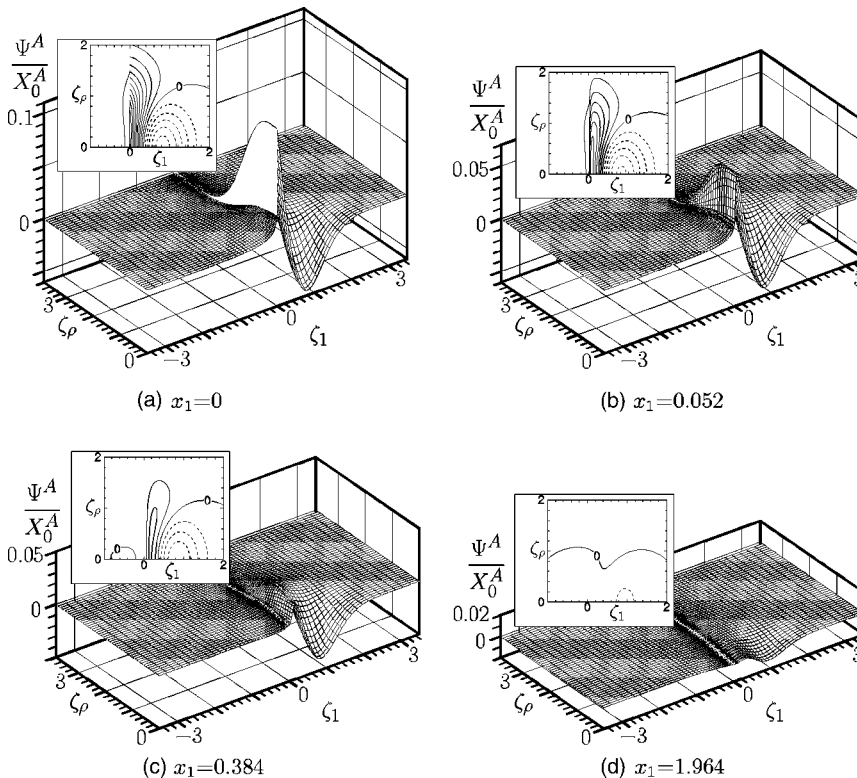


FIG. 7. Reduced velocity distribution function Ψ^A/X_0^A of species A and its contour plots for $m^B/m^A=5$ and $X_0^A=0.5$. (a) $x_1=0$, (b) $x_1=0.052$, (c) $x_1=0.384$, and (d) $x_1=1.964$. In the contour plots the curves are drawn with the interval of 0.01. The contour of positive values of Ψ^A is indicated by a solid line and that of negative values of Ψ^A by a dashed line.

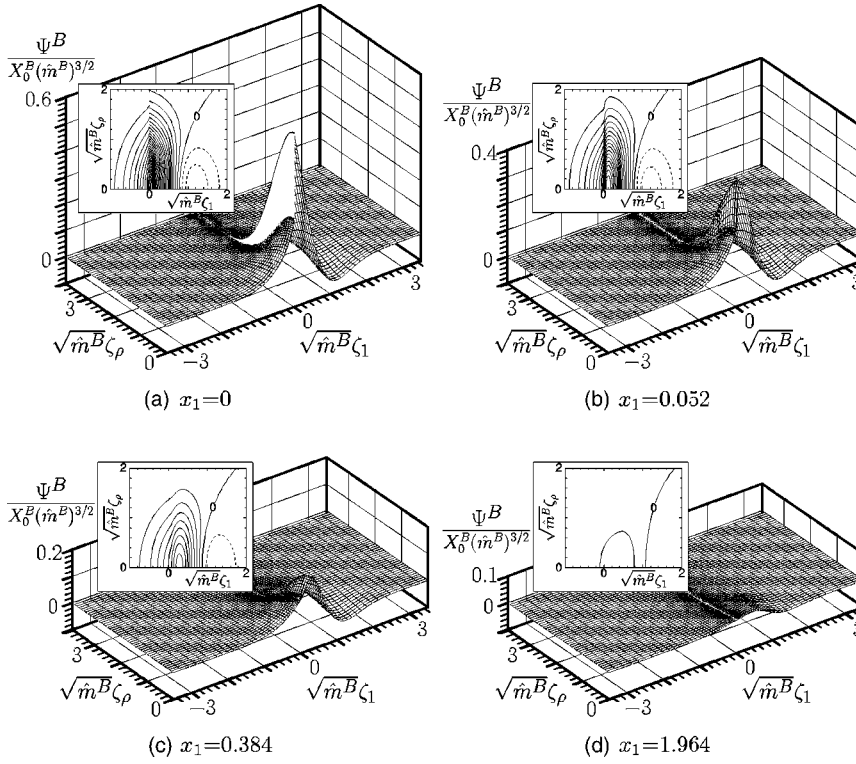


FIG. 8. Reduced velocity distribution function $\Psi^B/X_0^B(\hat{m}^B)^{3/2}$ of species B and its contour plots for $m^B/m^A=5$ and $X_0^A=0.5$. (a) $x_1=0$, (b) $x_1=0.052$, (c) $x_1=0.384$, and (d) $x_1=1.964$. In the contour plots the curves are drawn with the interval of 0.02. The contour of positive values of Ψ^B is indicated by a solid line and that of negative values of Ψ^B by a dashed line.

program of the Ministry of Education, Culture, Sports, Science and Technology, Japan).

APPENDIX A: COLLISION INTEGRALS

The collision integrals $L^{\beta\alpha}$ can be written in the form

$$L^{\beta\alpha}(f, g) = L_1^{\beta\alpha}(f) + L_2^{\beta\alpha}(g) - L_3^{\beta\alpha}(f) - \nu^{\beta\alpha}(|\zeta|)g, \quad (\text{A1})$$

where

$$L_J^{\beta\alpha}(f) = E^\alpha \int_0^\infty d\xi_\rho \int_{-\infty}^\infty d\xi_1 K_J^{\beta\alpha}(\xi_1, \xi_\rho, \zeta_1, \zeta_\rho) f(\xi_1, \xi_\rho) \quad (J = 1, 2, 3), \quad (\text{A2a})$$

$$\nu^\alpha(\zeta) = \frac{1}{2\sqrt{2}} \left[\frac{1}{\sqrt{\hat{m}^\alpha}} \exp(-\hat{m}^\alpha \zeta^2) + \left(2\zeta + \frac{1}{\hat{m}^\alpha \zeta} \right) \int_0^{\sqrt{\hat{m}^\alpha} \zeta} \exp(-y^2) dy \right]. \quad (\text{A2b})$$

The integral kernels $K_J^{\beta\alpha}$ are of the following form:

$$K_1^{\beta\alpha} = \begin{cases} \sqrt{\frac{2}{\pi}} \left(\frac{\hat{\mu}_-^{\beta\alpha}}{\hat{\mu}_-^{\alpha\beta}} \right)^2 \xi_\rho J_1^{\beta\alpha}(\xi_1, \xi_\rho, \zeta_1, \zeta_\rho) & \text{if } \hat{m}^\alpha \neq \hat{m}^\beta, \\ K_2^{\beta\alpha} & \text{if } \hat{m}^\alpha = \hat{m}^\beta, \end{cases} \quad (\text{A3a})$$

$$K_2^{\beta\alpha} = \left(\frac{\pi}{2} \hat{m}^\alpha \hat{m}^\beta \right)^{1/2} (\hat{\mu}_-^{\beta\alpha})^{-2} \xi_\rho e^{\hat{m}^\alpha |\zeta|^2} J_2^{\beta\alpha}(\xi_1, \xi_\rho, \zeta_1, \zeta_\rho), \quad (\text{A3b})$$

$$K_3^{\beta\alpha} = \sqrt{2\pi} \xi_\rho [(\xi_1 - \zeta_1)^2 + (\xi_\rho + \zeta_\rho)^2]^{1/2} E(k), \quad (\text{A3c})$$

with

$$J_1^{\beta\alpha} = \int_0^\pi d\varphi_\xi |\xi - \zeta| I_1^{\beta\alpha}(\xi_1, \xi_\rho, \varphi_\xi, \zeta_1, \zeta_\rho), \quad (\text{A4a})$$

$$J_2^{\beta\alpha} = \int_0^\pi d\varphi_\xi \frac{1}{|\xi - \zeta|} I_2^{\beta\alpha}(\xi_1, \xi_\rho, \varphi_\xi, \zeta_1, \zeta_\rho), \quad (\text{A4b})$$

$$I_1^{\beta\alpha} = e^{-a^{\beta\alpha}} \int_0^1 dt \cosh(-a^{\beta\alpha} t) \times \int_0^{\pi/2} ds \cosh(b^{\beta\alpha} \sqrt{1-t^2} \sin s), \quad (\text{A4c})$$

$$I_2^{\beta\alpha} = \exp\left(-\frac{\hat{m}^\beta}{4} \left(\frac{\hat{m}^\alpha}{\hat{m}^\beta} |\xi - \zeta| + \frac{|\zeta|^2 - |\xi|^2}{|\xi - \zeta|} \right)^2 \right), \quad (\text{A4d})$$

and

$$a^{\beta\alpha} = (\hat{\mu}_-^{\beta\alpha})^2 \left(\frac{|\xi|^2}{2\hat{m}^\alpha} + \frac{|\zeta|^2}{2\hat{m}^\beta} - \frac{\xi \cdot \zeta}{\hat{\mu}_-^{\beta\alpha}} \right), \quad (\text{A5a})$$

$$b^{\beta\alpha} = -\hat{\mu}_-^{\beta\alpha} |\xi \times \zeta|, \quad (\text{A5b})$$

$$\hat{\mu}_-^{\beta\alpha} = \frac{2\hat{m}^\beta \hat{m}^\alpha}{\hat{m}^\beta - \hat{m}^\alpha} \quad \text{for } \hat{m}^\beta \neq \hat{m}^\alpha, \quad (\text{A5c})$$

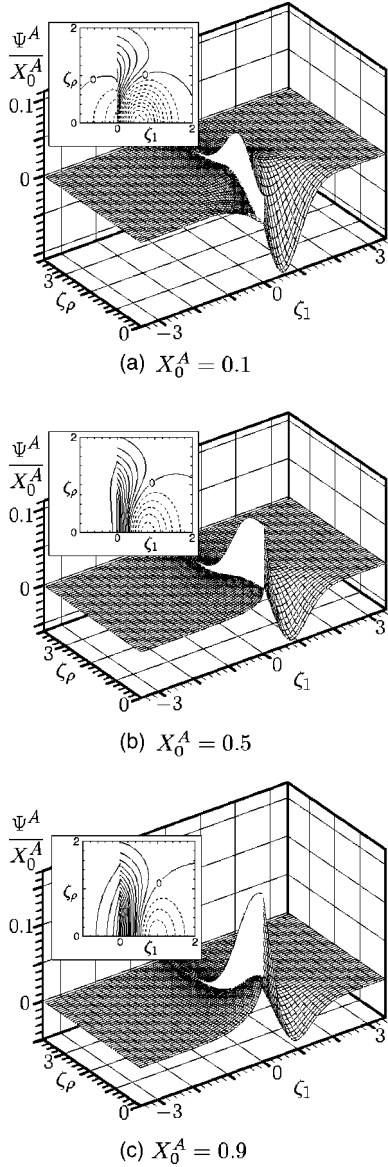


FIG. 9. Reduced velocity distribution function Ψ^A/X_0^A of species A and its contour plots at the surface of the condensed phase $x_1=0$ for $m^B/m^A=5$. (a) $X_0^A=0.1$, (b) $X_0^A=0.5$, and (c) $X_0^A=0.9$. See the caption of Fig. 7.

$$k = \frac{4\xi_\rho\zeta_\rho}{(\xi_1 - \zeta_1)^2 + (\xi_\rho + \zeta_\rho)^2}. \quad (\text{A5d})$$

The function E in Eq. (A3c) is the complete elliptic integral of the second kind⁴⁸ defined by

$$E(k) = \int_0^{\pi/2} (1 - k \sin^2 \theta)^{1/2} d\theta. \quad (\text{A6})$$

In the above expressions, the absolute values of vectors and the inner product of ξ and ζ are expressed in terms of ζ_1 , ζ_ρ , ξ_1 , ξ_ρ , and φ_ξ as follows:

$$|\xi - \zeta| = (|\xi|^2 + |\zeta|^2 - 2\xi \cdot \zeta)^{1/2}, \quad (\text{A7a})$$

$$|\xi \times \zeta| = [|\xi|^2|\zeta|^2 - (\xi \cdot \zeta)^2]^{1/2}, \quad (\text{A7b})$$

$$|\xi|^2 = \xi_1^2 + \xi_\rho^2, \quad |\zeta|^2 = \zeta_1^2 + \zeta_\rho^2, \quad (\text{A7c})$$

$$\xi \cdot \zeta = \xi_1\zeta_1 + \xi_\rho\zeta_\rho \cos \varphi_\xi. \quad (\text{A7d})$$

APPENDIX B: DATA OF COMPUTATION

We summarize the data of computation in this appendix.

- (i) In the present paper, we use the lattice systems generated by Eq. (34) in Ref. 14 for x_1 and by Eq. (53) in Ref. 13 for $\zeta_1\zeta_\rho$ plane. To be specific, in addition to the systems $\overline{S1-S4}$ for x_1 and $\overline{M1-M8}$ for $\zeta_1\zeta_\rho$ plane in the references, we use one system for x_1 , which we call $\overline{S5}$, and two systems for $\zeta_1\zeta_\rho$ plane, which we call $\overline{M9}$ and $\overline{M10}$. The system $\overline{S5}$ is defined by Eq. (34) in Ref. 14 with $\overline{N}_x = N_x = 800$. The system $\overline{M9}$ is defined by Eq. (53) in Ref. 13 with $\overline{Z}_1 = \overline{Z}_\rho = 4.5$, $\overline{N}_1 = 25$, $\overline{N}_\rho = 18$, $N_1 = 26$, and $N_\rho = 21$. The system $\overline{M10}$ is defined by the same equation with $\overline{Z}_1 = \overline{Z}_\rho = 4.5$, $\overline{N}_1 = 28$, $\overline{N}_\rho = 30$, $N_1 = 28$, and $N_\rho = 30$.
- (ii) Comparisons among the results for different lattice systems were made for $m^B/m^A=2$. A part of the results are shown in Table X. Here we summarize the main information about the lattice systems. For $\overline{S1}$, $\overline{S2}$, and $\overline{S5}$, the x_1 space is commonly truncated at $x_1=24.08$ ($d=24.08$), and there are 301, 601, and 801 points, respectively. System $\overline{S4}$ is the same as $\overline{S1}$ in the region

TABLE X. Comparisons of the coefficients γ^A , γ^B , and δ among different lattice systems for $m^B/m^A=2$. Comparisons were made at $X_0^A=0, 0.3, 0.7$, and 1.

Lattice systems	Maximum relative error		
	γ^A	γ^B	δ
$(\overline{S1}, \overline{M8})$ vs $(\overline{S4}, \overline{M8})$	7.4×10^{-7}	4.8×10^{-7}	1.7×10^{-6}
$(\overline{S1}, \overline{M8})$ vs $(\overline{S1}, \overline{M9})$	5.6×10^{-7}	4.8×10^{-7}	2.5×10^{-6}
$(\overline{S1}, \overline{M8})$ vs $(\overline{S2}, \overline{M8})$	1.7×10^{-6}	2.7×10^{-6}	1.9×10^{-6}
$(\overline{S1}, \overline{M8})$ vs $(\overline{S1}, \overline{M5})$	1.8×10^{-6}	1.8×10^{-6}	8.1×10^{-6}
$(\overline{S1}, \overline{M8})$ vs $(\overline{S1}, \overline{M3})$	3.7×10^{-6}	4.1×10^{-6}	3.6×10^{-5}
$(\overline{S1}, \overline{M1})$ vs $(\overline{S1}, \overline{M3})$	1.1×10^{-6}	1.2×10^{-6}	5.8×10^{-6}
$(\overline{S1}, \overline{M1})$ vs $(\overline{S1}, \overline{M2})$	2.0×10^{-6}	2.1×10^{-6}	6.2×10^{-6}
$(\overline{S1}, \overline{M1})$ vs $(\overline{S5}, \overline{M10})^a$	8.3×10^{-7}	1.5×10^{-6}	2.8×10^{-6}

^aA comparison was made at $X_0^A=0.3, 0.7$, and 1 for this case.

$0 \leq x_1 \leq 24.08$ and covers a wider region ($0 \leq x_1 \leq 32.49$) with 341 points. For $M1-M3$, $M5$, $M8$, and $M10$, the velocity space is commonly truncated at $|\zeta_1| = \zeta_\rho = 4.5/\sqrt{\hat{m}^\alpha}$ ($Z_1 = Z_\rho = 4.5$), and there are 101×55 , 101×73 , 101×49 , 113×37 , 101×37 , and 113×61 points, respectively. System $M9$ is the same as $M8$ in the region $-4.5 \leq \sqrt{\hat{m}^\alpha} \zeta_1 \leq 4.5$ and $0 \leq \sqrt{\hat{m}^\alpha} \zeta_\rho \leq 4.5$ and covers a wider region ($-5.06 \leq \sqrt{\hat{m}^\alpha} \zeta_1 \leq 5.06$ and $0 \leq \sqrt{\hat{m}^\alpha} \zeta_\rho \leq 5.25$) with 105×43 points. The comparisons in the table are made to assess the appropriate size of the lattice intervals and that of the truncation region. For example, the comparison between $(S1, M8)$ and $(S4, M8)$ is made for an estimate of the appropriate value of d . Similarly the comparison between $(S1, M8)$ and $(S1, M9)$ is made for an estimate of the appropriate values of Z_1 and Z_ρ . The comparison between $(S1, M8)$ and $(S2, M8)$ is for determining the number of lattice points in x_1 . The comparisons among $(S1, M1)$, $(S1, M2)$, $(S1, M3)$, $(S1, M5)$, and $(S1, M8)$ are for determining the number of points in $\zeta_1 \zeta_\rho$ plane. After such a series of tests, the system $(S1, M1)$ is chosen for $m^B/m^A=2$ and $(S4, M1)$ is chosen for $m^B/m^A=4, 5$, and 10 as the standard lattice system. The comparison between the standard system $(S1, M1)$ and the finest system $(S5, M10)$ are also shown for reference in Table X.

- (iii) Since we newly constructed the numerical kernel in the present work, we carried out several tests to assess the accuracy of the computation of the collision integrals. Here we show the results for the standard lattice system $M1$. First, we check the fundamental properties of the linearized collision integrals for the collision invariants: $L^{\beta\alpha}(g^\beta E^\beta, g^\alpha E^\alpha) = 0$ for $g^\alpha = 1, \hat{m}^\alpha \zeta_1, \hat{m}^\alpha |\zeta|^2$. The computed $|L^{\beta\alpha}(g^\beta E^\beta, g^\alpha E^\alpha)|$ is not exactly zero because the error comes from the part $L_1^{\beta\alpha} + L_2^{\beta\alpha} - L_3^{\beta\alpha}$ [see Eq. (A1); ν^β can be computed exactly because the integral in Eq. (A2b) is the error function]. The maximum value of $|L^{\beta\alpha}(g^\beta E^\beta, g^\alpha E^\alpha)|$ relative to the maximum of $|g^\alpha E^\alpha \nu^\beta|$ is bounded by 2.5×10^{-5} for $g^\alpha = 1$, 5.1×10^{-5} for $g^\alpha = \hat{m}^\alpha \zeta_1$, and 7.1×10^{-5} for $g^\alpha = \hat{m}^\alpha |\zeta|^2$, except for the case $m^B/m^A=10$ with $\alpha=A$ and $\beta=B$. For this case, the maximum is bounded by 5.5×10^{-5} , 9.3×10^{-5} , and 1.3×10^{-4} for $g^\alpha = 1, \hat{m}^\alpha \zeta_1$, and $\hat{m}^\alpha |\zeta|^2$, respectively. Second, we consider functions $A^\alpha(|\zeta|)$, $B^\alpha(|\zeta|)$, and $D^{(\beta)\alpha}(|\zeta|)$ that are the solutions for the following integral equations:

$$\sum_{\beta=A,B} K^{\beta\alpha} X_0^\beta L^{\beta\alpha} (\zeta_1 A^\beta E^\beta, \zeta_1 A^\alpha E^\alpha) + \zeta_1 (\hat{m}^\alpha |\zeta|^2 - \frac{\zeta}{2}) E^\alpha = 0, \quad (\text{B1})$$

$$\sum_{\beta=A,B} K^{\beta\alpha} X_0^\beta L^{\beta\alpha} (\zeta_{11} B^\beta E^\beta, \zeta_{11} B^\alpha E^\alpha) + 2\hat{m}^\alpha \zeta_{11} E^\alpha = 0, \quad (\text{B2})$$

$$\sum_{\beta=A,B} K^{\beta\alpha} X_0^\beta X_0^\alpha L^{\beta\alpha} (\zeta_1 D^{(\gamma)\beta} E^\beta, \zeta_1 D^{(\gamma)\alpha} E^\alpha) + \zeta_1 \left(\delta_{\alpha\gamma} - \frac{\hat{m}^\alpha X_0^\alpha}{\sum_{\beta=A,B} \hat{m}^\beta X_0^\beta} \right) E^\alpha = 0, \quad (\text{B3})$$

with subsidiary conditions

$$\sum_{\beta=A,B} \hat{m}^\beta X_0^\beta \int_0^\infty \zeta^4 A^\beta(\zeta) E^\beta(\zeta) d\zeta = 0,$$

$$\sum_{\beta=A,B} \hat{m}^\beta X_0^\beta \int_0^\infty \zeta^4 D^{(\alpha)\beta}(\zeta) E^\beta(\zeta) d\zeta = 0,$$

where $\zeta_{11} = \zeta_1^2 - \frac{1}{3} |\zeta|^2$, $\delta_{AA} = \delta_{BB} = 1$, $\delta_{AB} = \delta_{BA} = 0$, and α and γ run from A to B . It is seen from the third equation that $D^\alpha = D^{(A)\alpha} - D^{(B)\alpha}$ satisfies the relation

$$\sum_{\beta=A,B} K^{\beta\alpha} X_0^\beta X_0^\alpha L^{\beta\alpha} (\zeta_1 D^\beta E^\beta, \zeta_1 D^\alpha E^\alpha) + \zeta_1 (\delta_{\alpha A} - \delta_{\alpha B}) E^\alpha = 0. \quad (\text{B4})$$

We computed the quantity on the left-hand side of Eqs. (B1), (B2), and (B4), which is theoretically zero, by the use of highly accurate data of the functions A^α , B^α , and $D^{(\beta)\alpha}$ obtained in Ref. 49. We denote these quantities by $LB1$, $LB2$, and $LB4$, respectively. The maximum of $|LB1|$, $|LB2|$, and $|LB4|$ relative to the maximum of the absolute value of the second term in the same equation, $|\zeta_1 (\hat{m}^\alpha |\zeta|^2 - \frac{\zeta}{2}) E^\alpha|$, $|2\hat{m}^\alpha \zeta_{11} E^\alpha|$, and $|\zeta_1 (\delta_{\alpha A} - \delta_{\alpha B}) E^\alpha|$, is bounded by 8.0×10^{-5} , 1.2×10^{-4} , and 2.1×10^{-4} , respectively, for $m^B/m^A=2, 4$, and 5 . For $m^B/m^A=10$, it is bounded by 1.8×10^{-4} , 4.0×10^{-4} , and 4.6×10^{-4} , respectively.

- (iv) As mentioned in Sec. III B, Eq. (27) provides another measure of accuracy. For the standard lattice systems, the values of $|S_1^A + S_1^B|$ and $|H^A + H^B|$, which are theoretically zero, are computed for the values of X_0^A indicated by a closed circle in Fig. 1. They are bounded as $|S_1^A + S_1^B| < 5.9 \times 10^{-6}$ and $|H^A + H^B| < 4.8 \times 10^{-6}$. See Fig. 6 and Table IX for the magnitude of the functions S_1^A and H^A .
- (v) For the same values of X_0^A as (iv), we compared the maximum values of $|\Psi^A(d, \cdot, \cdot)|$, $|\Psi^\alpha(\cdot, \pm Z_1^\alpha, \cdot)|$, and $|\Psi^\alpha(\cdot, \cdot, Z_\rho^\alpha)|$ to the maximum value of $|\Psi^\alpha|$, where $Z_1^\alpha = Z_1/\sqrt{\hat{m}^\alpha}$ and $Z_\rho^\alpha = Z_\rho/\sqrt{\hat{m}^\alpha}$. The former three values should be negligible in order that the computation in the finite region of $(x_1, \zeta_1, \zeta_\rho)$ is justified. The results are

$$\frac{|\Psi^A(d, \cdot, \cdot)|}{\max|\Psi^A|} < \begin{cases} 3.5 \times 10^{-6} & (m^B/m^A = 2, 10), \\ 1.9 \times 10^{-7} & (m^B/m^A = 4, 5), \end{cases}$$

$$\frac{|\Psi^B(d, \cdot, \cdot)|}{\max|\Psi^B|} < \begin{cases} 4.9 \times 10^{-7} & (m^B/m^A = 2, 10), \\ 3.2 \times 10^{-8} & (m^B/m^A = 4, 5), \end{cases}$$

$$\frac{\max(|\Psi^A(\cdot, \pm Z_1^A, \cdot)|, |\Psi^A(\cdot, \cdot, Z_\rho^A)|)}{\max|\Psi^A|} < 5.9 \times 10^{-8},$$

$$\frac{\max(|\Psi^B(\cdot, \pm Z_1^B, \cdot)|, |\Psi^B(\cdot, \cdot, Z_\rho^B)|)}{\max|\Psi^B|} < 1.7 \times 10^{-8}.$$

- (vi) The accuracy of the Chebyshev polynomial approximation with respect to X_0^A was checked. The coefficients γ^A , γ^B , and δ obtained by the formula (34) with the data $\gamma^{A(n)}$, $\gamma^{B(n)}$, and $\delta^{(n)}$ in Tables I–III are compared with those computed directly. The comparison was made at common six sample values of X_0^A indicated by an open circle in Fig. 1. The relative errors to the directly computed data are less than 3.5×10^{-7} .

¹In the case of gas mixtures, the constitutive equation for the diffusion velocity is also necessary. In the present paper, we call the set of the convection-diffusion-type equations including this equation the Navier–Stokes set.

²These jumps are different from those on the surface of a simple rigid solid body in a slightly rarefied gas. The former is finite under the ordinary pressure, while the latter vanishes. See also the last paragraph in the Introduction.

³M. N. Kogan, “Kinetic theory in aerothermodynamics,” *Prog. Aerosp. Sci.* **29**, 271 (1992).

⁴T. Ytrehus, “Molecular-flow effects in evaporation and condensation at interfaces,” *Multiphase Sci. Technol.* **9**, 205 (1997).

⁵Y. Sone, “Kinetic theoretical studies of the half-space problem of evaporation and condensation,” *Transp. Theory Stat. Phys.* **29**, 227 (2000).

⁶Y. Sone, *Kinetic Theory and Fluid Dynamics*, Modeling and Simulation in Science, Engineering and Technology (Birkhäuser, Boston, 2002).

⁷V. I. Roldughin and V. M. Zhdanov, “Non-equilibrium thermodynamics and kinetic theory of gas mixtures in the presence of interfaces,” *Adv. Colloid Interface Sci.* **98**, 121 (2002).

⁸K. Aoki, S. Takata, and S. Taguchi, “Vapor flows with evaporation and condensation in the continuum limit: effect of a trace of noncondensable gas,” *Eur. J. Mech. B/Fluids* **22**, 51 (2003).

⁹Y. Sone and Y. Onishi, “Kinetic theory of evaporation and condensation—Hydrodynamic equation and slip boundary condition,” *J. Phys. Soc. Jpn.* **44**, 1981 (1978).

¹⁰Y. Onishi and Y. Sone, “Kinetic theory of slightly strong evaporation and condensation—Hydrodynamic equation and slip boundary condition for finite Reynolds number,” *J. Phys. Soc. Jpn.* **47**, 1676 (1979).

¹¹K. Aoki and Y. Sone, “Gas flows around the condensed phase with strong evaporation or condensation: Fluid dynamic equation and its boundary condition on the interface and their application,” in *Advances in Kinetic Theory and Continuum Mechanics*, edited by R. Gatignol and Soubbaramayer (Springer, Berlin, 1991), p. 43.

¹²S. Takata “Diffusion slip for a binary mixture of hard-sphere molecular gases: Numerical analysis based on the linearized Boltzmann equation,” in *Rarefied Gas Dynamics*, edited by T. J. Bartel and M. A. Gallis (AIP, Melville, NY, 2001), p. 22

¹³S. Takata, S. Yasuda, S. Kosuge, and K. Aoki, “Numerical analysis of thermal-slip and diffusion-slip flows of a binary mixture of hard-sphere molecular gases,” *Phys. Fluids* **15**, 3745 (2003).

¹⁴S. Yasuda, S. Takata, and K. Aoki, “Numerical analysis of the shear flow of a binary mixture of hard-sphere gases over a plane wall,” *Phys. Fluids* **16**, 1989 (2004).

¹⁵Y. Sone, T. Ohwada, and K. Aoki, “Temperature jump and Knudsen layer in a rarefied gas over a plane wall: Numerical analysis of the linearized Boltzmann equation for hard-sphere molecules,” *Phys. Fluids A* **1**, 363 (1989).

¹⁶Y. Sone, K. Aoki, and I. Yamashita, “A study of unsteady strong condensation on a plane condensed phase with special interest in formation of steady profile,” in *Rarefied Gas Dynamics*, edited by V. Boffi and C.

Cercignani (Teubner, Stuttgart, 1986), Vol. II, p. 323.

¹⁷Y. Sone, K. Aoki, H. Sugimoto, and T. Yamada, “Steady evaporation and condensation on a plane condensed phase,” *Theor Appl. Mech.* **19** (3), 89 (1988).

¹⁸Y. Sone and H. Sugimoto, “Strong evaporation from a plane condensed phase,” in *Adiabatic Waves in Liquid-Vapor Systems*, IUTAM Symposium, Göttingen, 1989, edited by G. E. A. Meier and P. A. Thompson (Springer, Berlin, 1990), p. 293.

¹⁹K. Aoki, K. Nishino, Y. Sone, and H. Sugimoto, “Numerical analysis of steady flows of a gas condensing on or evaporating from its plane condensed phase on the basis of kinetic theory: Effect of gas motion along the condensed phase,” *Phys. Fluids A* **3**, 2260 (1991).

²⁰Y. Sone, F. Golse, T. Ohwada, and T. Doi, “Analytical study of transonic flows of a gas condensing on its plane condensed phase on the basis of kinetic theory,” *Eur. J. Mech. B/Fluids* **17**, 277 (1998).

²¹S. Ukai, T. Yang, and S.-H. Yu, “Nonlinear boundary layers of the Boltzmann equation: I. Existence,” *Commun. Math. Phys.* **236**, 373 (2003).

²²S. Ukai, T. Yang, and S.-H. Yu, “Nonlinear stability of boundary layers of the Boltzmann equation, I. The case $M^\infty < -1$,” *Commun. Math. Phys.* **244**, 99 (2004).

²³Y. Sone, “Kinetic theory of evaporation and condensation—Linear and nonlinear problems,” *J. Phys. Soc. Jpn.* **45**, 315 (1978).

²⁴S. Takata, “Half-space problem of weak evaporation and condensation of a binary mixture of vapors,” in *Rarefied Gas Dynamics*, edited by M. Capitelli (AIP, New York, in press).

²⁵J. W. Cipolla, Jr., H. Lang, and S. K. Loyalka, “Temperature and partial pressure jumps during evaporation and condensation of a multicomponent gas mixture,” in *Rarefied Gas Dynamics*, edited by M. Becker and M. Fiebig (DFLR, Porz-Wahn, 1974), Vol. II, F. 4.

²⁶I. V. Volkov and V. S. Galkin, “Analysis of temperature jump and partial pressure coefficients of a binary evaporating gas mixture,” *Fluid Dyn.* **26**, 914 (1991).

²⁷Y. Onishi, “Kinetic theory analysis for temperature and density fields of a slightly rarefied binary gas mixture over a solid wall,” *Phys. Fluids* **9**, 226 (1997).

²⁸As far as the linearized problem, which will be studied here (see the next paragraph), is concerned, the present setting that there is no tangential flow at a far distance is most general. Even if one starts with the (superficial) general setting of flow velocity as $(u_{1\infty}, u_{2\infty}, u_{3\infty})$, no tangential flow $u_{2\infty} = u_{3\infty} = 0$ is concluded because of the existence and uniqueness theorem to be described in Sec. III A. In contrast, for the nonlinear problem, it is not the case, and one has to consider the nonzero tangential flow in general.

²⁹M. N. Kogan, *Rarefied Gas Dynamics* (Plenum, New York, 1969).

³⁰S. Chapman and T. G. Cowling, *The Mathematical Theory of Non-Uniform Gases*, 3rd ed. (Cambridge University Press, Cambridge, 1995).

³¹J. O. Hirschfelder, C. F. Curtiss, and R. B. Bird, *Molecular Theory of Gases and Liquids* (Wiley, New York, 1954).

³²K. Aoki, C. Bardos, and S. Takata, “Knudsen layer for gas mixtures,” *J. Stat. Phys.* **112**, 629 (2003).

³³H. Grad, “Singular and nonuniform limits of solutions of the Boltzmann equation,” in *Transport Theory*, edited by R. Bellman, G. Birkhoff, and I. Abu-Shumays (AMS, Providence, RI, 1969), p. 269.

³⁴N. B. Maslova, “Kramers problem in the kinetic theory of gases,” *USSR Comput. Math. Math. Phys.* **22**, 208 (1982).

³⁵C. Bardos, R. E. Caflisch, and B. Nicolaenko, “The Milne and Kramers problems for the Boltzmann equation of a hard sphere gas,” *Commun. Pure Appl. Math.* **39**, 323 (1986).

³⁶C. Cercignani, “Half-space problems in the kinetic theory of gases,” in *Trends in Applications of Pure Mathematics to Mechanics*, edited by E. Kröner and K. Kirchgässner (Springer, Berlin, 1986), p. 35.

³⁷F. Coron, F. Golse, and C. Sulem, “A classification of well-posed kinetic layer problems,” *Commun. Pure Appl. Math.* **41**, 409 (1988).

³⁸F. Golse and F. Poupaud, “Stationary solutions of the linearized Boltzmann equation in a half-space,” *Math. Methods Appl. Sci.* **11**, 483 (1989).

³⁹Y. Sone, T. Ohwada, and K. Aoki, “Evaporation and condensation on a plane condensed phase: Numerical analysis of the linearized Boltzmann equation for hard-sphere molecules,” *Phys. Fluids A* **1**, 1398 (1989).

⁴⁰C. Gasquet and P. Witomski, *Fourier Analysis and Applications* (Springer, New York, 1999).

⁴¹The definition of β_i in (34) in Ref. 25 would be wrong. In the present comparison, we used the formulas (38) and (39) in Ref. 25 with $\beta_i = m_i/2kT_0$.

⁴²A. Frezzotti, “Kinetic theory description of the evaporation of multi-

- component substances,” in *Rarefied Gas Dynamics*, edited by C. Shen (Peking University Press, Beijing, 1997), p. 837.
- ⁴³Y. Sone and S. Takata, “Discontinuity of the velocity distribution function in a rarefied gas around a convex body and the S layer at the bottom of the Knudsen layer,” *Transp. Theory Stat. Phys.* **21**, 501 (1992).
- ⁴⁴S. Takata, “Kinetic theory analysis of the two-surface problem of a vapor-vapor mixture in the continuum limit,” *Phys. Fluids* **16**, 2182 (2004).
- ⁴⁵Y. Sone, K. Aoki, S. Takata, H. Sugimoto, and A. V. Bobylev, “Inappropriateness of the heat-conduction equation for description of a temperature field of a stationary gas in the continuum limit: Examination by asymptotic analysis and numerical computation of the Boltzmann equation,” *Phys. Fluids* **8**, 628 (1996); **8**, 841(E) (1996).
- ⁴⁶Y. Sone, “Flows induced by temperature fields in a rarefied gas and their ghost effect on the behavior of a gas in the continuum limit,” *Annu. Rev. Fluid Mech.* **32**, 779 (2000).
- ⁴⁷A. V. Bobylev, “Quasistationary hydrodynamics for the Boltzmann equation,” *J. Stat. Phys.* **80**, 1063 (1995).
- ⁴⁸M. Abramowitz and I. A. Stegun, *Handbook of Mathematical Functions* (Dover, New York, 1968).
- ⁴⁹S. Takata, S. Yasuda, K. Aoki, and T. Shibata, “Various transport coefficients occurring in binary gas mixtures and their database,” in *Rarefied Gas Dynamics*, edited by A. D. Ketsdever and E. P. Muntz (AIP, New York, 2003), p. 106.